Deciphering post-caldera volcanism: insight into the Vulcanello (Island of Vulcano, Southern Italy) eruptive activity based on geological and petrological constraints

Raffaella Fusillo[1], Federico Di Traglia[2], Anna Gioncada[3]*, Marco Pistolesi[2], Paul J. Wallace[4], Mauro Rosi[3]

1. Department of Earth Sciences, University of Bristol, Wills Memorial Building, Queen's Road, BS8 1RJ Bristol, United Kingdom
2. Dipartimento di Scienze della Terra, Università di Firenze, Via La Pira 4, 50121 Firenze, Italy
3. Dipartimento di Scienze della Terra, Università di Pisa, Via Santa Maria 53, 56126 Pisa, Italy
4. Department of Geological Sciences, University of Oregon, Eugene, OR 97403, USA

*corresponding author: anna.gioncada@unipi.it

Keywords: Post-caldera volcanism; Melt inclusions; Shoshonitic volcanism; Aeolian Archipelago.

Abstract

Integrated field-based volcanology and petrologic studies can provide relevant clues about the way in which structural features, magma replenishment of a shallow sub-caldera reservoir, and magma evolution exert control on eruption behavior during post-caldera volcanism. Post–caldera activity of the past 1000 yrs at the La Fossa caldera (Island of Vulcano, Italy), occurred at two vents: the dominantly explosive La Fossa vent located at the center of the caldera and the lava-dominated Vulcanello vent located close to the northern ring fault of the caldera. Revised chrono-stratigraphic data indicate that the activity occurred in two clusters of eruptions: in the 11th-12th centuries and during the 17th century. The activity was in part contemporaneous with La Fossa vent and led to the formation of three, partially overlapped strombolian cones. Each cone-building episode was accompanied by the outpouring of lava in subaerial and submarine environments. The erupted volumes of the pyroclastic cones vary between $2x10^{-3}$ km^3 and $3x10^{-6}$ km^3, while the volumes of the three lavas span between 0.3 km^3 (a submarine lava field) and $3x10^{-3}$ km^3. Petrology data indicate that the activity of Vulcanello was fed by three different magma batches: Vulcanello 1 was fed by a slightly zoned reservoir of shoshonitic composition, Vulcanello 2 was fed by a slightly more evolved magma whereas Vulcanello 3 was fed by latitic magma. The compositions of melt inclusions (major elements and volatile content) trapped in olivine separated from pyroclastic materials record the entire differentiation history and suggest that all Vulcanello magmas underwent volatile loss during pre-eruption equilibration at ≤1 km depth. Integration of all available information also suggests that in the last 1000 yrs the northern caldera fault acted as a preferential duct for the rise of degassed magma from the sub-caldera magma reservoir whereas volatile release namely took place separately at La Fossa cone where activity was almost entirely explosive in nature.

Introduction

Post-caldera volcanism reflects the evolution of residual magma evolution and/or magma chamber replenishment episodes in the period following caldera collapse (Druitt et al. 2012) and it is generally controlled by the geometric and kinematic features of ring-faults (Geyer and Martì 2014). This work is aimed at understanding magma intrusion and migration leading to the onset of the eruptive activity at post-caldera volcanoes. We choose as a case study the Vulcanello peninsula, a ring-fault volcano located in the northern part of La Fossa caldera (Island of Vulcano; Fig. 1), by analysing the stratigraphic sequence along with geomorphologic and petrological studies.

Geological Setting

The Island of Vulcano (Aeolian Islands, Southern Italy) consists of several volcanic edifices whose formation overlapped in time and space beginning 120 ka (Keller 1980; Lanza & Zanella 2003; De Astis et al. 2013 and references therein). The composite volcanic system comprises the Primordial Vulcano edifice (120–100 ka), dissected by the development of Il Piano caldera around 100 ka and subsequently by the La Fossa caldera (80 ka to 15 ka) (Keller 1980; Gioncada and Sbrana 1991). Over the past 15 ka, in the northern sector of the island (Keller 1980), several vents were activated in a N–S direction (Saraceno, La Fossa cone, Faraglione, Vulcanello). This alignment can also be traced towards the near Lipari island, which was characterized in some cases by contemporaneous volcanic activity (Gioncada et al. 2003; Forni et al. 2013). The two most recent volcanoes are La Fossa, a 391-m-high, active composite cone that began to erupt around 5.5 ka according to Frazzetta et al. (1984), and Vulcanello, a small volcanic peninsula to the north (Fig. 1). The Vulcanello peninsula, a 123-m-high, composite edifice showing three coalescent crater rims, is composed of a lava platform and three partially overlapping scoria cones aligned NE–SW along the northern ring fault of La Fossa caldera (Ventura et al. 1999; Blanco-Montenegro et al. 2007; Davì et al. 2009; De Astis et al. 2013; Romagnoli et al. 2013). Vulcanello erupted shoshonitic to latitic products, with

latite characterizing the last cycle of activity (Keller 1980; De Astis et al. 1997; Davì et al. 2009). The onset of the Vulcanello activity is still a matter of debate. Some Authors (Keller 1970, 1980; Voltaggio et al. 1995; De Astis et al. 2013) suggest that the early activities of Vulcanello may have occurred in 126 or 183 BC, as reported by the Strabo and Plinius historical chronicles quoted by Mercalli and Silvestri (1891) and De Fiore (1922), mainly based on radiometric ages and on the presence of the AD 776 M. Pilato tephra layer from Lipari Island above the Vulcanello lava platform (Keller 1980; De Astis et al. 2013) (Table 1). By contrast, Arrighi et al. (2006), based on archaeomagnetic studies, suggest that the Vulcanello lava platform was built up during a continuous volcanic activity which occurred from AD 1100 to 1250 (Table 1). This latter hypothesis is also supported by recent studies (Tanguy et al. 2003; Zanella 2006; Davì et al. 2009; Gurioli et al. 2012; Di Traglia et al. 2013) evidencing that the exotic tephra layer from the Island of Lipari overlying the Vulcanello lava platform can be attributed to the explosive phase of the Rocche Rosse eruption (the Rocche Rosse tephra, Cortese et al. 1986; Dellino and La Volpe 1995) representing the most recent phases of activity on Lipari (AD 1220). Forni et al. (2013) suggest that on Lipari island the Rocche Rosse, included within the Vallone Fiume Bianco Synthem, was characterized by a complex sequence of explosive phases that mostly produced a succession of fallout, lithic-rich pumiceous lapilli-tuffs, with minor interlayered beds of lapill-tuffs with accretionary lapilli deposited from dilute pyroclastic density currents which heralded the emission of a final lava coulee. Archeomagnetic dating on the coulee (Tanguy et al. 2003) and fission track age (Bigazzi et al. 2003) on a coeval pyroclastic sequence (Lami succession) suggest the AD 1220 as the most probable age for the Rocche Rosse eruptive sequence. In agreement, the Rocche Rosse tephra was found on Vulcano island interbedded with the Breccia di Commenda eruption deposit (Gurioli et al. 2012; Di Traglia et al. 2013), dated using paleomagnetic methods on lithic clast by Gurioli et al. (2012) at AD 918–1302, and thus consistent with the AD 1230±40 archeomagnetic dating of Arrighi et al. (2006) of the Vulcanello platform and with the 0.61±0.02 cal ka BP (ca. AD 1335) ^{14}C dating of Caron et al. (2012) on cryptotephra found in a marine core from the Northern Ionian Sea.

Recently, a new stratigraphic reconstruction of the volcaniclastic succession of the last 1000 years of activity at La Fossa (Di Traglia et al. 2013) subdivided the stratigraphic record into two main units, namely the Palizzi–Commenda (PCEC) and Gran Cratere (GCEC) eruptive clusters. The Eruptive Cluster (EC) represents a series of eruptions clustered in time and forming a stratigraphic unit that is hierarchically higher than an Eruptive Unit but lower than an Eruptive Epoch (de Rita et al., 1998; Di Traglia et al. 2013); it is defined as a unit that is bounded by unconformities (erosional surfaces and/or palaeosols) and extends over a wide area (at least the cone and the surrounding plains and valleys). The oldest eruptive cluster (PCEC), comprising the Palizzi (PEU) and Commenda (CEU) eruptive units, occurred in the 13th century according to ages from Arrighi et al. (2006) and Gurioli et al. (2012), in a very short time compared to previous reconstructions. Archeomagnetic age and the identification of the Rocche Rosse tephra and the Pal B rhyolitic layer related to the PEU on top of the Vulcanello platform agree well with the onset of sub-aerial activity of Vulcanello close in time to the reactivation of the La Fossa cone in the late Middle Ages (~AD 1200) (Arrighi et al. 2006; Gurioli et al. 2012; Di Traglia et al. 2013; Table 1).

A larger consensus exists for timing of the products related to the last explosive activity (Vulcanello 3) emplaced above a paleosol dated at 0.397 + 0.097 ka (i.e. 17th century; Keller 1980). The isthmus linking Vulcanello and the rest of Vulcano island (Vulcano Porto plain; Fig. 1) began to develop after the emplacement of the Vulcanello lava platform (post-12th century AD; Arrighi et al. 2006; Di Traglia et al. 2013).

Data

Field data collection was carried out during different surveys starting from 2008. Forty natural sections were integrated with six machine-excavated and hand-dug pit trenches (Fig. 2). Morphological analysis and volume calculations for the Vulcanello peninsula were performed by integrating direct field observations with data from the DTM. Major element compositions of the juvenile clasts and volatile concentrations of olivine-hosted melt inclusions (MI) were measured in

quenched products of Vulcanello explosive activity. We also analysed glass samples from the submarine effusive activity NE of Vulcanello (pillow lava). Methodological techniques are detailed in the electronic supplementary material.

Stratigraphy and Eruptive Units

The entire stratigraphic sequence of Vulcanello activity has been divided into three lithosomes (Vulcanello 1, Vulcanello 2 and Vulcanello 3); a comparison with previous reconstructions is shown in Table 2. A lithosome is an informal stratigraphic unit defined by lithological and morphological elements having a combination that defines a genetically homogeneous rock body, corresponding to a well-defined volcanic edifice with a recognizable morphology related to a defined eruptive centre (Giordano et al. 2006). In a map, a lithosome defines a stratigraphically and morphologically recognizable volcanic center (Tibaldi 2010). Each lithosome, which also marks a change of eruptive vent, is separated by erosive unconformities (e.g., the unconformable basal contact of a volcanic pile, the structural-morphological surface resulting from a caldera collapse) that are linked genetically to the evolution of the volcano (Palladino et al. 2010). Different from other stratigraphic units, lithosomes do not imply any hierarchic degree (Palladino et al. 2010). Within each lithosome, several eruptive (comprising both lavas and pyroclastic deposits) and epiclastic units (comprising deposits not directly related to eruptions; Manville et al. 2009) have been identified, separated by unconformities of lower rank compared to those between the lithosomes. Eleven eruptive units and three epiclastic units have been recognized: five eruptive units and two epiclastic units within Vulcanello 1, one eruptive unit and one epiclastic unit within Vulcanello 2, and six eruptive units within Vulcanello 3.

A synthetic log of the tephra units and lava flow deposits identified in the Vulcanello area and studied in this work (Fig. 3; Table 3) integrates the tephra sequence observed on the cones and on the lava plateau. The stratigraphic relationships between Vulcanello deposits and La Fossa and

Rocche Rosse (Lipari) deposits on the Vulcanello platform are exemplified in Fig. 4, using logs of selected natural outcrops and machine-excavated and hand-dug pit trenches.

Vulcanello 1 Lithosome

We identified five eruptive Units which correspond to the stratigraphic sequence of Vulcanello 1 Lithosome. The Vulcanello 1A Unit is characterized by two different lithofacies (the Plateau Lava and the Grey Pyroclastics, Table 3, Fig. 5a, b). The Plateau Lava (Fig. 5a) is composed by several massive lava flows, often showing columnar jointing and ropy pahoehoe surfaces. The Grey Pyroclastics are well exposed at the sea-cliff in the eastern side (outcrops 26, 27 in Fig. 2) of the Vulcanello 1 cone, where they form a 9 m-thick, grain-supported, massive to stratified deposit. A 50 cm-thick volcanoclastic unit overlies the Vulcanello 1A deposits, indicating a short eruptive rest. This unit is in turn overlain by a massive lapilli deposit (Vulcanello 1B); on the eastern side of the cones (outcrops 26, 27 in Fig. 2), Vulcanello 1B is represented by a 3 m-thick, greenish, grain-supported, fine to coarse lapilli, normal to reversely graded deposit. A thin (15 cm) volcanoclastic unit separates Vulcanello 1B from Vulcanello 1C, which in turn outcrops in the eastern and southern side of the cones (outcrops 23, 24, 26, 27 in Fig. 2) as a 5 m-thick, normally-graded, lapilli to bomb-sized deposit. A 9 m-thick spatter deposit (Vulcanello 1D, Fig. 5c) closes the Vulcanello 1 Lithosome. The entire stratigraphic sequence is cut by a feeding dyke observable within the eastern sea-cliff (Fig. 5b).

Vulcanello 2 Lithosome

A time break between Vulcanello 1 and the overlying Vulcanello 2 Lithosome is marked by a stratigraphic erosional unconformity and by the presence of a reworked deposit (maximum thickness 2 m; Fig. 6a). Vulcanello 2 is composed of a single Eruptive Unit (Vulcanello 2, Table 3), which outcrops on the north-eastern cliff (outcrop 26 in Figs. 2a, 4) and in the southern flank of the cones (outcrop 22 in Fig. 2), where it forms a 3 m-thick fallout deposit characterized by a lower

massive part grading upward into a normal-reversely graded deposit (Fig. 6a). The explosive activity of Vulcanello 2 is possibly associated with the intrusion of the dyke that cuts all the products of Vulcanello 1 and with the emplacement a submarine lava field offshore of the northeastern side of Vulcanello (Gamberi et al. 1997; Gamberi 2001; Romagnoli et al. 2013). Vulcanello 1 and Vulcanello 2 lithosomes are covered by the Pal B rhyolitic layer (Figs. 6, 7), by the Rocche Rosse tephra (Fig. 8) and by the ash fraction of the Commenda deposit (Figs. 7, 8, 9).

Vulcanello 3 Lithosome

A paleosol dated at 0.397 + 0.097 ka (Keller 1980; De Astis et al. 2013) separates Vulcanello 2 from Vulcanello 3 Lithosome which comprises 6 eruptive units (Table 3). The lower unit (Vulcanello 3A) corresponds to a fine-grained, grey to black stratified ash deposit that opens the Vulcanello 3 activity (Fig. 9). This unit has been identified only in machine-made trenches and on the cliff on the northern sector, directly overlying the Rocche Rosse tephra from Lipari. Vulcanello 3A is overlain by the Vulcanello 3B lava (the Roveto Lava described by Keller 1980; Fig. 9a) which was emitted from the northwestern part of the cones and flowed in E-W direction. Being clearly exposed only within the crater walls and below the water tank located at the foot of the cone (outcrop 11 in Fig. 2a), the source area of Vulcanello 3B lava is unclear. The lava is overlain by a pyroclastic sequence which comprises three main tephra units (Vulcanello 3C, 3D and 3E; Fig. 9b, c, d). Vulcanello 3C outcrops in the north-western side (outcrops 11, 12, 13 in Fig. 2a) as a 3 m-thick, stratified, ash to lapilli deposit. It has been also found in some trenches on the lava platform (trenches 29, 30, 31 in Fig. 2). Vulcanello 3C is overlain by the Vulcanello 3D Unit, consisting of a 3 m-thick, massive to normally-graded, grain-supported lapilli deposit (Fig. 9b; outcrop 14 in Fig. 2a). A fine ash-rich, thinly laminated, 3m-thick deposit (Vulcanello 3E; Fig. 9) overlies Vlo3D on the crater-rim (outcrop 15 in Fig. 2a), on the cone flanks and in some trenches (29, 30, 31 Fig. 2a; Fig. 9). No juvenile clasts are clearly identifiable within this final deposit.

A final lava flow (Vulcanello 3F), which flowed in the same direction of Vulcanello 3B, closes the eruptive sequence of Vulcanello 3; although the Roveto lava flow, (Vulcanello 3B in our reconstruction, has been previously classified as a single unit (Davì et al. 2009; De Astis et al. 2013), we suggest that at least two different flows were emplaced. No clear geometric relationships exist on the cone, but the observations made along the sea cliff and the lack of the tephra sequence covering Vulcanello 3B lava flow on top of the final lava suggest the existence of two different lava flows.

Morphological analysis and erupted volumes

The Vulcanello peninsula can be divided into two main geomorphological domains: the cone complex and the lava platform. The cone complex comprises three cones truncated by three craters. The transition from the crater rim to the cone flanks is marked by a change in slope from 5° to 30°. The cone flanks are dominated mainly by sheet erosion, while slope failures occur in the eastern sector. The Vulcanello cone complex is a constructional landform, as revealed by its high height (H)/base area (Wb) ratio (H/Wb = 0.76); the summit area (Ws)/base area ratio (Ws/Wb = 0.46) indicates that it is slightly irregular in shape. The edifice has a conical form with an elliptical base, and the summit area is characterised by ESE–WSW striking major axes. The main destructive features are the three crater structures truncating the summit of the cone and the landslide scar that cuts the first cone in its eastern margin (Keller 1980; Romagnoli et al. 2013).

The lava platform consists of several lobes, which originate from the cone area (Fig. 2). The more evident lobe corresponds to the Valle dei Mostri lava that flowed in a NNE direction from the boundary between the second and the third cone.

The volume of erupted products is defined by the volume of the Vulcanello peninsula (cones complex, lava platform and Roveto + Valle dei Mostri lava flows) and the volume of the submarine lava field (Gamberi et al. 1997; Gamberi 2001; Romagnoli et al. 2013). The volumes (Dense Rock Equivalent, DRE; Table 4) of the three cones vary between $2x10^{-3}$ km^3 for the first cone and $3x10^{-6}$

km^3 for the third cone, while the volumes of the three lavas vary between 0.345 (submarine lava field, considering 3.5 km^2 and 70 m the area distribution and the average thickness) (Romagnoli et al. 2013) and $3x10^{-3}$ km^3 (Roveto + Valle dei Mostri lava flows). Vulcanello emplaced the maximum erupted volume during the Vulcanello 2 Lithosome activity, with the emplacement of a very large submarine lava flow field. The erupted lava volume/total volume ratio varies between 0.93 (Vulcanello 1 Lithosome) and 0.99 (Vulcanello 2 and 3 Lithosomes), implying that the explosivity decreased in time, with the more explosive activity being related to Vulcanello 1. The average growth rate of the cone in the last 1000 years is therefore 0.28 km^3 ky^{-1}, lower than the value of 0.96 km^3 ky^{-1} estimated for the La Fossa cone (Di Traglia et al. 2013). It is worth noting that if only the cone volume is used as representative of the eruptive activity, this introduces an error between 5% and 20% in the volume calculation (Di Traglia et al. 2009; Rodriguez-Gonzales et al. 2010; Cimarelli et al. 2013).

Petrography and whole rock compositions

The samples of Vulcanello tephra selected for melt inclusion analyses have shoshonitic and latitic compositions when classified on a K_2O vs SiO_2 wt% diagram, and contain from 53 to 58 wt% SiO_2 (Fig. 10; Table 5). The pillow lava of Vulcanello 2 has shoshonitic composition.

Geochemical and petrologic studies of Vulcanello rocks have mostly focused on lava samples (e.g. Davì et al. 2009, with 20 lava samples and 3 scoria and bomb samples; see also De Astis et al. 2013 and references therein). Our data on the pyroclastic products agree with the previous data in indicating shoshonitic composition for the Vulcanello 1 and Vulcanello 2 Lithosomes and latitic composition for the Vulcanello 3 Lithosome (Fig. 10). Davì et al. (2009) reported a shoshonitic composition for a bomb sampled at the base of Vulcanello 3 piroclastic deposits. As regards the shoshonitic rocks, the Vulcanello 2 tephra has lower MgO and Fe_2O_3t and higher Al_2O_3 and CaO with respect to Vulcanello 1A and B, suggesting higher olivine fractionation. The composition of

the shoshonitic tephra samples is silica-undersaturated, with normative nepheline up to 10%, while the latites are only slightly undersaturated (Table 5).

Overall, the primary mineral assemblage of tephra and lava products consists of clinopyroxene, plagioclase, olivine, and Fe-Ti oxides both in the shoshonitic and latitic products, with a relative decrease of olivine and the appearance of sanidine in the phenocryst assemblage of the latites. Leucite is also a common groundmass/microphenocryst phase in the shoshonites.

The lava units analysed for the three different lithosomes (Vulcanello 1 Plateau Lava, Vulcanello 2 dyke and submarine lava and Vulcanello 3 Lavas) display different petrographic characteristics.

The Plateau Lavas show clinopyroxene, olivine and plagioclase phenocrysts and magnetite in a groundmass made of the same minerals, sanidine and leucite. Clinopyroxene is predominant in phenocrysts and microphenocrysts.

The dyke is petrographically similar to the plateau lava, except for the lack of small-sized plagioclase and the acicular/skeletal shape of clinopyroxene microphenocrysts, suggestive of a rapid growth event before the final groundmass crystallization. The rounded shape of the large plagioclase crystals contrasts with the euhedrality of mafic minerals.

Similar textures of the phenocrysts and microphenocrysts are visible in the pillow lavas, differing only for the glassy groundmass: clinopyroxene was rapidly crystallizing immediately before the eruption, while plagioclase lacks evidence of rapid crystallization and shows rounded corners. Opaques (magnetite) and apatite are accessories. The glassy brown groundmass shows sporadic clinopyroxene microlites.

The Vulcanello 3 lavas have phenocrysts of clinopyroxene, strongly zoned plagioclase with antirapakiwi texture and minor sanidine, olivine and opaques. Rounded xenocrysts of quartz and of minerals largely replaced by opaques are frequent. Rounded and sieve-textured plagioclase crystals characterize the Roveto lava, similarly to the shoshonitic dyke. The groundmass is dominated by feldspars. The Valle dei Mostri lava flow differs from the Roveto lava in the moderately higher phenocryst abundance and in the vesicular and partially oxidized groundmass.

Melt inclusions

Melt inclusion morphological features

Melt inclusion (MI) shape, relationship with the host-crystal, texture and the presence of vapor bubbles and microlites were inspected as they unravel processes of inclusion formation and post-entrapment modification. Most of the MI in Vulcanello olivine have spherical/sub–spherical shape and aphyric brown transparent glass (Fig. 11a, b, c), except those, finely crystallized, from the Grey Pyroclastics deposit of the Vulcanello 1A Unit. The eighteen MI analysed have a size that ranges from 87 μm (V3D5) to 605 μm (V1C5) and are 'fully–enclosed' (Cervantes and Wallace 2003), that is they can only communicate with the external melt by diffusion through the host crystal. None contains microlites.

Two MI out of eighteen have a 'wrinkled' texture along the inclusion–host interface (Fig. 11A). The wrinkled texture is similar to that observed in melt inclusions that have been experimentally reheated, as a result of a rapid dissolution of olivine. In the natural melt inclusions this textural feature may form due to magma mixing (Cervantes and Wallace 2003). The lack of shrinkage bubbles (Fig. 11; Roedder 1984) suggests very little change in temperature between the time the inclusions were originally trapped and the time of eruption, and that cooling during eruption was relatively rapid (Wallace et al. submitted). Theoretical and experimental studies (Lowenstern 1994; Tait 1992) confirm that rapid cooling allows MI to quench without bubble formation.

Major element composition of melt inclusions and submarine glass samples

The measured major element composition of MI is reported in Table 6 together with the volatile content and the host crystal forsterite content, which was analysed close to the MI. Details on data collection and number of analyses are reported in the Appendix.

The forsterite content of olivine phenocrysts ranges from $Fo_{64,5}$ to $Fo_{70,2}$ (Table 6). The low forsterite content is consistent with the low Mg# (Mg#= MgO/(MgO+FeOt)) of the MI (Table 6),

suggesting that their compositions were not strongly modified by post-entrapment crystallization of olivine along the inclusion walls. The correlation of the CaO/Al_2O_3 (incompatible elements in olivine) vs MgO ratio of the Vulcanello melt inclusions (not shown), also suggests that the melt inclusions have not been strongly affected by boundary layer enrichment processes (Métrich and Wallace 2008). To correct for any effects of post-entrapment crystallization, we added 0.1% increments of equilibrium olivine, calculated using Fe-Mg partitioning (Roeder and Emslie 1970), to the composition of each inclusion until equilibrium with the host was achieved. The composition of each MI corrected for post-entrapment crystallization is reported in Table 6. All inclusions required less than 2 wt% of olivine addition to restore equilibrium, and some of them did not require any (Table 6). Therefore, the fractionation trend within V1C melt inclusion group reflects entrapment of melts with different evolution degree and not post-entrapment crystallization of the host.

The MI have, after correction, SiO_2 contents that range from 51.5 wt% in V1C to 61.9 wt% in V3D (Table 6). The composition of the glass samples from Vulcanello 2 submarine lava nearly overlaps that of the melt inclusions in olivine of Vulcanello 2 explosive activity (Table 7; Fig. 12).

In a K_2O vs SiO_2 diagram (Fig. 12), the MI composition plots in the field of the Vulcanello and La Fossa products from Gioncada et al. (1998). When compared with the bulk rock analyses in variation diagrams (Fig. 12), the composition of MI shows similar trends with initial increase of Al_2O_3 and decrease of MgO, CaO, FeOt, TiO_2 and subsequent decrease of the same elements including Al_2O_3. These trends correspond to those already recognized in Vulcanello and La Fossa eruptive products (Del Moro et al., 1998; De Astis et al. 1997, 2013). The major element composition of the MI, therefore, indicates that they are representative of the compositions of the different magma batches that fed the activity of Vulcanello during its entire history.

Volatiles in melt inclusions and pressure of entrapment

The H_2O concentrations in MI from Vulcanello's explosive activity, corrected for post-entrapment olivine crystallization, are ≤1 wt%, with average values (± 1σ) of 0.68 ± 0.31 wt% for Vulcanello 1, 0.57± 0.23 wt% for Vulcanello 2, and 0.56± 0.35 wt% for Vulcanello 3 (Table 6; Fig. 12). The highest H_2O concentrations are recorded in Vulcanello 1 (V1C) with values up to 1.32 wt%, matching with the highest concentration of sulphur (Fig. 12). The chlorine dissolved in MI increases with the magmatic evolution, while the sulfur content decreases (Fig. 12). Fluorine concentration, on the contrary, is constant (Fig. 12). The H_2O dissolved in submarine glass samples is on average lower (0.36 wt%) than that in MI.

Using the H_2O concentration it is possible to estimate vapour saturation pressures and therefore the minimum pressure of entrapment or last equilibration (Anderson et al. 1989). All the analysed MI were fully enclosed without vapour bubble, therefore suitable for entrapment pressure estimates (Cervantes and Wallace 2003). The saturation pressure was assessed on the basis of the empirical H_2O solubility model of Moore et al. (1998), using the corrected MI composition and a temperature of 1100°C from microthermometric results (Gioncada et al. 1998). The values obtained range from 0.2 MPa to a maximum of 21.2 MPa (Table 6). On the basis of a geobaric gradient of 27.5 MPa/km for a continental crust average density of 2.8 g/cm^3, the minimum depth of entrapment/last equilibration is lower than 1 km beneath the volcano.

Discussion

Reconstruction of the eruptive activity

The data reported support our interpretation that the activity forming the early sub-aerial part of Vulcanello (Vulcanello 1 Lithosome) started in the XI-XII centuries AD as proposed by Arrighi et al. (2006), with emplacement of the lava platform (Vulcanello 1A Plateau Lava) which comprises several superimposed lava flows with a total volume of 2.6×10^{-2} km^3. The effusive activity was coeval with explosive activity (Vulcanello 1A Grey Pyroclastics, 1B, 1C, 1D) which formed a cinder cone with a volume of 2×10^{-3} km^3. We infer that emergence of the Vulcanello islet

represented the final stage of growth through the accumulation of pillow lavas erupted in submarine environments and presently recognized along the north-eastern submarine slopes of the islet (Gamberi and Marani 1997; Romagnoli et al. 2013) and accompanied by explosive activity at the surface, as reported in historical accounts (Mercalli and Silvestri 1891, De Fiore 1922).

After a short time break marked by deposition of intercalated epiclastic deposits within the tephra sequence, the activity resumed with explosive eruptions (Vulcanello 2) which led to the formation of a second cone (total volume of 1.5×10^{-4} km^3). The recognition of the rhyolitic pumice from La Fossa cone (Pal B; Fig. 4) and of the Rocche Rosse tephra from Lipari on top of the Vulcanello 2 Lithosome (Di Traglia et al. 2013) suggest that the beginning of the Vulcanello activity was close in time to the reactivation of the La Fossa cone in the late Middle Ages (~AD 1200).

About five centuries of rest followed, before activity of Vulcanello resumed with the emplacement of a latitic lava flow (Vulcanello 3B, Roveto lava flow) with a total volume of 3×10^{-3} km^3, heralded by an initial phase of explosive activity (Vulcanello 3A). In some previous reconstructions (Davì et al., 2009), Vulcanello 3B is attributed to the final stage of Vulcanello 2 activity, but based on its relationship with the ash found below the lava, we consider Vulcanello 3B as part of the Vulcanello 3 cycle. The lava emission was followed by three explosive phases (Vulcanello 3C, 3D and 3E) that led the edification of the third cone with a volume of 2.5×10^{-3} km^3. The first of these events (Vulcanello 3C) had a strong phreatic signature, with no or little magma involvement. The emission of strongly altered lithic material after the emplacement of the Roveto lava flow, coupled to the intense alteration affecting the Roveto lava outcrops close to the crater area, suggest that, in a relatively short period of rest, the intense magmatic degassing of the shallow magma batch induced hydrothermal circulation and consequent alteration in the area of the Vulcanello 3 crater. The Vulcanello 3C phreatic phase was followed by the Vulcanello 3D explosive activity, having a clear magmatic origin. Instead, the following explosive phase (Vulcanello 3E) which formed the upper part of the cone was again dominated by altered material giving a definite reddish colour to the ash deposits. The activity of Vulcanello 3 was closed by the emplacement of a final lava (Vulcanello

3F) which mostly flowed in the same direction of the Roveto lava. The presence of a second cluster of eruptions was also confirmed by historical accounts, which described frequent eruptive activity at Vulcanello, La Fossa cone and Forgia craters during the XVII-XVIII centuries (Mercalli and Silvestri 1891; De Fiore 1922). Moreover, the deposits related to the activity of Vulcanello 3 are coeval with the lower part of the GCEC (Di Traglia et al. 2013). On the basis of historical chronicles and stratigraphic reconstructions, we can thus infer that during this period multiple vents were active at the Island of Vulcano. The behaviour of Vulcanello resembles that of La Fossa cone, with several eruptions not equally-spaced but mostly clustered in time. Clusters of eruptions have been identified at several mafic-to-intermediate central volcanoes, such as Cotopaxi (Pistolesi et al. 2011), Vesuvius (Arrighi et al. 2001; Principe et al. 2004), Etna (Branca and Del Carlo 2005; Allard et al. 2006) and at mafic volcanic fields (Garrotxa Volcanic Field; Cimarelli et al. 2013) and are related to the interplay between tectonic stress and variable magma supply from depth (Takada 1999).

The overall Vulcanello eruption rate (i.e. the eruption rate during the entire cycle of the volcano) is estimated at 0.28 km^3 kyr^{-1}; if considering only the Vulcanello 1 and 2 lithosomes, the average eruption rate rises to 1.37 km^3 kyr^{-1}. For comparison, the eruption rate of the nearby La Fossa cone is within this range (0.96 km^3 kyr^{-1}; Di Traglia et al. 2013) implying that Vulcanello was fed by short-lived magma batches (10^2–10^3 years), as also proposed by Hobden et al. (2002) for the Ngauruhoe volcano (New Zealand), which is characterized by a comparable growth rate (0.9 km^3 kyr^{-1}).

Geochemical and petrological constraints for the Vulcanello shallow storage system

The magmas erupted at Vulcanello register an appreciable, although modest, differentiation range (Davì et al. 2009; De Astis et al. 2013; this work). The least differentiated magmas were the shoshonites erupted in Vulcanello1 phase, fed by a slightly zoned magma batch, with the most evolved magmas erupted first. The magmas of Vulcanello 2 phase were only slightly more evolved

than those of Vulcanello 1, while during Vulcanello 3 phase the erupted magmas were definitely the most differentiated at Vulcanello.

The comparison of the chemical composition of the melt inclusions from Vulcanello explosive activity with the bulk rock data available on lavas and tephra indicates that MI can be confidently considered representative of the different magma batches that fed the volcanic activity of Vulcanello (Fig. 12). Therefore, the MI record the entire differentiation history of Vulcanello magmas.

The largely spherical shapes of the melt inclusions in all the studied samples, together with the euhedral shape of the olivine host crystals, suggest low cooling rates on the order of 1 to 2°C/h (Métrich and Wallace 2008) and rule out the growth of olivine under strong undercooling conditions during rapid magma ascent. The crystallization, therefore, occurred during the pre-eruptive storage of each magma batch, having progressively more evolved composition.

The volatile content of Vulcanello MIs can be used to assess the degassing history and the last magma storage depth. On the basis of MI textural features, it can be inferred that their low content of H_2O (0.36 wt% - 1.32 wt%), and their sulfur, chlorine and fluorine content (100-500 ppm, 2800-4100 ppm, 1200-1900 ppm, respectively) are representative of the pre-eruptive volatile budget. The CO_2 content is below the detection limit (50 ppm). Due to its low solubility, CO_2 tends to degas almost entirely before significant H_2O is lost. The lack of measurable CO_2 in Vulcanello MIs is in agreement with previous data indicating that CO_2 is exsolved deep below Vulcano (Gioncada et al. 1998).

Loss of H_2O from MI due to hydrogen diffusion through the host commonly occurs during magma ascent, in order to reach equilibrium with the outer melt (Chen et al. 2011; 2013; Bucholz et al. 2013; Lloyd et al. 2013). However, on the basis of the comparison of the radius of Vulcanello MI (~70 μm) and the olivine size (0.7 – 0.5 mm) with the results of Chen et al. (2013), and the fact that MI were selected far from the host rim, it is unlikely that water loss by hydrogen diffusion affected

significantly the studied MI. Therefore, the measured volatile content is likely to be representative of the saturation pressure of a magma batch equilibrated at about 1 km beneath the volcano.

Previous works (Zanon et al. 2003; Peccerillo et al. 2006) identified for the Vulcanello feeding system a 20 km-deep mafic magma storage level, close to the Moho, and a shallower reservoir located at 3-5 km, related to a lithological boundary between the metamorphic basement and the base of the volcanic complex. An additional magma reservoir at 1.3 km was identified below La Fossa (Clocchiatti et al. 1994a).

The MI textural and analytical data obtained in this work indicate for Vulcanello a period of magma residence at about 1 km of depth, suggesting a similarity of the plumbing system with La Fossa cone. Although all the analysed MI were trapped at shallow depths, the Vulcanello 1 shoshonites may still signal the ascent of magma from deeper storage (Vetere et al. 2007; Davì et al. 2009).

The latter cluster of Vulcanello eruptive episodes occurred after magma differentiation to latite and concomitant with development of shallow hydrothermal alteration. Passive degassing at Vulcanello, as well as at La Fossa cone (Fulignati et al. 1998; Carapezza et al. 2011), can be the result of magma storage and evolution in a shallow reservoir fed by a deeper system (Clocchiatti et al. 1994b). During the differentiation of shoshonite to latite, sulfur and water were lost through open-system degassing at shallow depth. Chlorine, in contrast, increased during differentiation from about 52 to 55-56 wt% SiO_2, indicating incompatible behaviour consistent with the low partitioning of chlorine in the aqueous fluid phase at low pressure. This behaviour mimics that observed at La Fossa (Clocchiatti et al. 1994b), confirming the similarities between these two volcanoes.

Vulcanello feeding system

Zanon et al. (2003) report that the Vulcanello activity provides evidence of the deepest (about 20 km) storage zone of the polybaric plumbing system that fed the island of Vulcano (Fig. 13). A shallower shoshonitic storage system located at depths of 3-5 km (Zanon et al. 2003; De Ritis et al. 2013) was then identified as the source of the primitive magmas which fed both Vulcanello and La

Fossa cone activity (Gioncada et al. 1998). Seismic data also suggests the existence of a seismogenic structure below Vulcanello, interpreted as a discontinuity linking the deep (21 km) reservoir to the magma accumulation zones at 3-5 km and representing the preferential pathway along which magma may move from the deep system to the intermediate storage zone (Gambino et al. 2012).

The Vulcanello transport system is probably tied to the northern ring fault of the La Fossa caldera (Ventura et al. 1999; Davì et al. 2009). We hypothesize that magma batches repeatedly intruded the ring fault structure, supplying the activity of the three Vulcanello lithosomes. Intrusion of magma along a ring fault depends on two driving mechanisms (Rubin 1995): i) the overcoming of the minimum principal stress ($\sigma 3$) by magmastatic pressure (main driving force until reaching the level of neutral buoyancy) (Takada et al. 1999) and ii) the magma overpressure component (crucial for the lateral expansion of dikes) (Rubin 1995). Moreover, ring-faults help sheet intrusions to reach the surface, providing an almost homogeneous (in term of stress field homogenization) pathway for reaching the surface (Browning and Gudmundsson 2014). If we consider that the magma ascent is only due to buoyancy, the magmastatic overpressure component p_e may be estimated using the relation (Vetere et al. 2007):

$$p_m = \Delta \rho g h \qquad (1)$$

where $\Delta\rho$ is the difference between the density of the country rock and the melt (average 335 kg/m^3; Vetere et al. 2007), g is the gravity, and h is the vertical length of the dike (3-5 km depth).

The obtained values are in the order of 10-16 MPa, within the range of magma overpressure in basaltic dikes (Becerril et al. 2013). For a volcano such as the La Fossa caldera, both the sheet dip and the geometry of the shallow magma chamber make the length of the sheet, L, greater than the depth of the magma chamber z (Gudmundsson 2011):

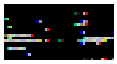

(2)

where α is the dip of the sheet (43° for the Vulcanello 2 feeder dike). The length of the sheet L ranges between 4 and 7 km and, given its geometry, sheet L could be defined as cone sheet (30–45°, inwardly dipping sheet intrusion; Walter and Troll 2001). Considering elongation of the Vulcanello 1 cone (500-700 m) as a proxy for the length (d) of the feeder sheet (the intersection between the sheet and the surface), we can evaluate the depth (h) of the magma chamber (Becerril et al. 2013):

$$h = \frac{\Delta u E}{2 d \Delta\rho (1-\nu^2)} - \frac{\rho m - \sigma_d}{g \Delta\rho} \qquad (3)$$

where E and v are the host rock Young's modulus and Poisson's ratio, respectively, and σ_d is the differential stress (the difference between the vertical stress and the minimum principal horizontal stress). The obtained value for the magma chamber depth is in the range 4-6 km, which agrees with previous estimates based on petrological data (Zanon et al. 2003).

The Vulcanello 2 feeder dike is NE-SW-oriented, in agreement with the direction of the La Fossa caldera ring-fault (Romagnoli et al. 2013), while the submarine lava field is aligned with the Vulcanello cones in a ENE-WSW direction. This implies that buoyant upward flow of the magma that fed the explosive activity rose along a cone sheet while the outward flow rose toward the ENE buttressed from the conduit, as it has been observed in other scoria cones (Petronis et al. 2013) and central volcanoes (Intrieri et al. 2013). Horizontally propagating intrusions can only be emplaced if the edifice load prevents eruption through the central area and if magma is negatively buoyant at shallow depth (Pinel and Jaupart 2004). In regard to the activity of Vulcanello 3 Lithosome, we hypothesize that the shoshonitic magma evolved to latite through fractionation and crustal assimilation at shallow depth, possibly about 1 km. Evidence of the very shallow magma storage and differentiation in the Vulcanello 3 activity is testified by the occurrence of altered materials ejected during phreatic activity and by an extensive fumarole field associated with the weathered zone in the northern side of the Vulcanello cones.

Vetere et al. (2007) calculated a magma rise speed in the range 0.089 m/s to 0.45 m/s for the Vulcanello eruptive system. This rise speed range falls within that of Strombolian to Hawaiian

activity (Parfitt 2004) and is consistent with the negligible water loss for hydrogen diffusion (Chen et al. 2013; Le Voyer et al. 2014). Considering the length of the feeding sheet and the rise speed, we infer an ascent time in the range 2-22 hours, in good agreement with the mixed effusive-explosive eruptive style (Scandone et al. 2007).

Concluding remarks

Few post-caldera volcanic crises have been monitored during their pre-eruptive phases such as at Rabaul (New Guinea) (Roggensack et al. 1996; Saunders 2001), Hudson (Chile) (Kratzmann et al. 2009; Delgado et al. 2014), Eyjafjallajökull (Iceland) (Sigmundsson et al. 2010; Tarasewicz et al. 2012), Ferdinandina (Galapágos) (Chadwick et al. 2011; Bagnardi et al. 2013), and therefore the eruptive behaviour of post-caldera volcanism is not well characterized. The integration of new stratigraphic, geomorphologic, geochemical, and petrological data with a revision of chrono-stratigraphic data allowed us to decipher the evolution of Vulcanello, a post-caldera volcano of the Island of Vulcano, located along the northern part of the La Fossa caldera ring fault.

The main outcomes can be summarized as follow:

- The onset of the Vulcanello activity is not unequivocally constrained. Early eruptions of Vulcanello may have occurred in 126 or 183 BC, as reported by the Strabo and Plinius historical chronicles quoted by Mercalli and Silvestri (1891) and De Fiore (1922). The sub-aerial part of Vulcanello could be considered as the final part of a submarine growth process that also involved sporadic sub-aerial activity spaced in time.
- The sub-aerial volcanic activity occurred in two clusters of eruptions. The first (AD 1100 to 1250; Arrighi et al. 2006) led to the construction of the main part of the peninsula, with the growth of two cones (Vulcanello 1 and 2 Lithosomes) associated with two lava flows (the Vulcanello platform lava and a submarine pillow lava field). The second cluster of eruptions built the third cone on the pre-existing Vulcanello 1 and 2 cones, after a period of

quiescence recorded by the presence of a paleosol (0.397 + 0.097 ka; Keller 1980). Four eruptive units were produced, in association with with the Roveto-Valle dei Mostri lava flows (Vulcanello 3 Lithosome). The occurrence of the second cluster of eruptions is also confirmed by historical accounts (De Fiore 1922).

- The erupted volumes (DRE) of the three cones range from $2x10^{-3}$ km^3 (Vulcanello 1 Lithosome) to $3x10^{-6}$ km^3 (Vulcanello 3 Lithosome), while the volumes of the three lavas vary between 0.34 (submarine lava field) and $3x10^{-3}$ km^3 (Roveto lava flows). The ratio of erupted lava volume to total volume varies from 0.93 (Vulcanello 1 Lithosome) to 0.99 (Vulcanello 2 and 3 Lithosomes), implying that explosivity decreased through time, with the more explosive activity related to Vulcanello 1. The average growth rate of the cone in the last 1000 years is estimated 0.28 km^3 ky^{-1}.
- The Vulcanello activity was fed by three different magma batches. The least differentiated magmas are represented by the shoshonites erupted in Vulcanello 1 Lithosome, fed by a slightly zoned magma batch, while the magmas of Vulcanello 3 were definitely the most differentiated at Vulcanello.
- The MI from deposits of Vulcanello explosive activity record the entire differentiation history of Vulcanello magmas. The MI volatile content indicates that the shoshonitic and latitic magmas last resided about 1 km beneath the volcano, suggesting a similarity with the La Fossa plumbing system.
- Rise of a shoshonitic magma from a deep storage system occurred at the onset of the Vulcanello eruptive activity. Magma migrated through the ring faults once magma overpressures reached 10-16 MPa along a 4-7 km-long, 43° dipping, NE-SW oriented cone sheet. Outgassing led to mixed effusive – weak explosive activity. Considering a magma rise speed of 0.089 - 0.45 m/s (Vetere et al. 2007) and the length of the feeding cone sheet, we estimated an ascent time in the range of 2-22 hours, in good agreement with the mixed effusive-explosive eruptive style (Scandone et al. 2007).

- The stratigraphic evidence of the contemporaneous, or almost so, activity at La Fossa cone (resurgent volcano) and Vulcanello (ring-fault volcano) during the last 1000 years (Di Traglia et al. 2013) suggest the need for further investigations in order to unravel possible relationships between the different post-caldera shallow storage systems. Notably, the two post-caldera centres, fed by the same deep magmatic system (Davì et al. 2009), have, in the last 1000 years, contrasting eruptive behavior, with La Fossa producing mostly explosive eruptions, while at Vulcanello degassed magma was generally effused. The study of MI from deposits of La Fossa eruptions that were contemporaneous or nearly so, based on stratigraphic evidence, to Vulcanello's activity will allow comparison of magma storage and ascent in the two systems, which will help us to fully understand their different eruptive behaviours. This approach (field-based volcanology joined to petrology) could give insights into post-caldera volcanism worldwide and, more specifically, support assessment of multiple-vent hazard scenarios at Vulcano.

References

Allard P, Behncke B, D'Amico S, Neri M, Gambino S (2006) Mt Etna 1993–2005: Anatomy of an evolving eruptive cycle. Earth-Science Reviews 78: 85–114 doi: 10.1016/j.earscirev.2006.04.002

Anderson AT Jr, Newman S, Williams S N, Druitt, TH, Skirius C, Stolper E (1989) H_2O, CO_2, Cl and gas in Plinian and ash flow Bishop rhyolite. Geology 17:221-225

Arrighi S, Tanguy JC, Rosi M (2006) Eruptions of the last 2200 years at Vulcano and Vulcanello (Aeolian Islands, Italy) dated by high-accuracy archeomagnetism. Phys Earth Plan Int 159:225-233

Bagnardi M, Amelung F, Poland MP (2013) A new model for the growth of basaltic shields based on deformation of Fernandina volcano, Galápagos Islands. Earth and Planetary Science Letters 377: 358-366

Becerril L, Galindo I, Gudmundsson A, Morales JM (2013) Depth of origin of magma in eruptions. Sci Rep 3:2762

Bigazzi G, Coltelli M, Norelli P (2003) Nuove eta` delle ossidiane di Lipari determinate con il metodo delle tracce di fissione. GeoItalia, 4th Forum FIST, Bellaria, 16–18 September, 444–446

Blanco-Montenegro I, De Ritis R, Chiappini M (2007) Imaging and modelling the subsurface structure of volcanic calderas with high-resolution aeromagnetic data at Vulcano (Aeolian Islands, Italy). Bull Volcanol 69:643-659

Branca S, Del Carlo P (2005) Types of eruptions of Etna volcano AD 1670–2003: implications for short-term eruptive behaviour. Bull Volcanol 67: 732–742

Browning J, Gudmundsson A (2014) Ring dykes as partially captured inclined sheets: insights from field observations and numerical modelling. EGU General Assembly Conference Abstracts 2014

Bucholz CE, Gaetani GA, Behn MD, Shimizu N (2013) Post-entrapment modification of volatiles and oxygen fugacity in olivine-hosted melt inclusions. Earth Planet Sci Lett 374:145-155

Carapezza ML, Barberi F, Ranaldi M, Riccia T, Tarchini L, Barrancos J, Fischer C, Perez N, Weber K, Di Piazza A, Gattuso A (2011) Diffuse CO_2 soil degassing and CO_2 and H_2S concentrations in air and related hazards at Vulcano Island (Aeolian arc, Italy). J Volcanol Geotherm Res 207:130–144

Caron, B., Siani, G., Sulpizio, R., Zanchetta, G., Paterne, M., Santacroce, R., Tema, E. & Zanella, E. (2012). Late Pleistocene to Holocene tephrostratigraphic record from the Northern Ionian Sea. Marine Geology 311:41-51

Cervantes P, Wallace P (2003) Magma degassing and basaltic eruption styles: a case study of 2000 year BP Xitle volcano in central Mexico. J Volcanol Geotherm Res 120:249-270

Chadwick Jr WW, Jónsson S, Geist DJ, Poland M, Johnson DJ, Batt S, Harpp KS, Ruiz A (2011) The May 2005 eruption of Fernandina volcano, Galápagos: The first circumferential dike intrusion observed by GPS and InSAR. Bull Volcanol 73:679-697

Chen Y, Provost A, Schiano P, Cluzel N (2011) The rate of water loss from olivine-hosted melt inclusions. Contrib Mineral Petrol 162:625-636

Chen Y, Provost A, Schiano P, Cluzel N (2013) Magma ascent rate and initial water concentration inferred from diffusive water loss from olivine-hosted melt inclusions. Contrib Mineral Petrol 165:525-541

Chiarabba C, Pino NA, Ventura G, Vilardo G (2004) Structural features of the shallow plumbing system of Vulcano Island Italy. Bull Volcanol (2004) 66:477–484 DOI 10.1007/s00445-003-0331-9

Cimarelli C, Di Traglia F, de Rita D, Torrente DG (2013) Space–time evolution of monogenetic volcanism in the mafic Garrotxa Volcanic Field (NE Iberian Peninsula). Bull Volcanol 75:1-18

Clocchiatti R, Del Moro A, Gioncada A, Joron JL, Mosbah M, Pinarelli L, Sbrana A (1994a) Assessment of a shallow magmatic system: The 1888–90 eruption, Vulcano Island, Italy. Bull Volcanol 56:466-486

Clocchiatti R, Gioncada A, Mosbah M, Sbrana A (1994b) Possible deep origin of sulphur output at Vulcano (Southern Italy) in the light of melt inclusion studies. Acta Vulcanologica 5: 49-54

Cortese M, Frazzetta G, La Volpe L (1986) Volcanic history of Lipari (Aeolian Islands, Italy) during the last 10,000 years. J Volcanol Geotherm Res 27: 117–133

Davì M, De Rosa R, Donato P, Vetere F, Barca D, Cavallo A (2009) Magmatic Evolution and plumbing system of ring-fault volcanism: the Vulcanello Peninsula (Aeolian Islands, Italy). Eur J Mineral 21:1009-1028

Davì M, De Rosa R, Donato P, Sulpizio R (2011). The Lami pyroclastic succession (Lipari, Aeolian Islands): A clue for unravelling the eruptive dynamics of the Monte Pilato rhyolitic pumice cone. J Volcanol Geotherm Res, 201:285-300.

De Astis G, Lucchi F, Dellino P, La Volpe L, Tranne CA, Frezzotti ML, Peccerillo A (2013) Geology, volcanic history and petrology of Vulcano (central Aeolian archipelago). Geol Soc London Mem 37:281-349

De Astis G, La Volpe L, Peccerillo A, Civetta L (1997) Volcanological and Petrological evolution of Vulcano Island (Aeolian Arc, Southern Tyrrenian Sea). J Geophys Res 102: 8021-8050

De Fiore O (1922) Vulcano (Isole Eolie). Riv Vulcanologica I. Friedlaender (Suppl. 3), 1–393

de Rita D, Giordano G, Milli S (1998) Forestepping-backstepping stacking patterns of volcaniclastic successions: Roccamonfina volcano, Italy. J Volcanol Geotherm Res 80:155–178

De Ritis R, Ravat D, Ventura G, Chiappini M (2013) Curie isotherm depth from aeromagnetic data constraining shallow heat source depths in the central Aeolian Ridge (Southern Tyrrhenian Sea, Italy). Bull Volcanol 75:1-11

Delgado F, Pritchard M, Lohman R, Naranjo J A (2014) The 2011 Hudson volcano eruption (Southern Andes, Chile): Pre-eruptive inflation and hotspots observed with InSAR and thermal imagery. Bull Volcanol 76:1-19

Dellino P, La Volpe L (1995) Fragmentation versus transportation mechanisms in the pyroclastic sequence of Monte Pilato-Rocche Rosse (Lipari, Italy). J Volcanol Geotherm Res 64:211–231

Del Moro A, Gioncada A, Pinarelli L, Sbrana A,, Joron JL (1998) Sr, Nd and Pb isotope evidence of open system evolution at Vulcano (Aeolian arc, Italy): Lithos 43:81-106 doi:10.1016/S0024-4937(98)00008-5

Di Traglia, F., Cimarelli, C., De Rita, D., Gimeno Torrente, D. (2009) Changing eruptive styles in basaltic explosive volcanism: Examples from Croscat complex scoria cone, Garrotxa Volcanic Field (NE Iberian Peninsula). Journal of Volcanology and Geothermal Research, 180(2), 89-109.

Di Traglia F, Pistolesi M, Rosi M, Bonadonna C, Fusillo R, Roverato M (2013) Growth and erosion: The volcanic geology and morphological evolution of La Fossa (Island of Vulcano, Southern Italy) in the last 1000years. Geomorphology 194:94-107

Di Traglia F, Morelli S, Casagli N, Garduño Monroy VH (2014) Semi-automatic delimitation of volcanic edifice boundaries: Validation and application to the cinder cones of the Tancitaro–Nueva Italia region (Michoacán–Guanajuato Volcanic Field, Mexico). Geomorphology 219:152-160

Dixon JE, Stolper EM, Holloway JR (1995) An experimental study of water and carbon dioxide solubilities in mid-ocean ridge basaltic liquids. Part I: calibration and solubility models. J Petrol 36:1607–1631

Druitt TH, Costa F, Deloule E, Dungan M, Scaillet B (2012) Decadal to monthly timescales of magma transfer and reservoir growth at a caldera volcano. Nature 482(7383):77-80

Fine G, Stolper E (1986) Dissolved carbon dioxide in basaltic glasses: concentrations and speciation. Earth Planet Sci Lett 76:263-278

Forni F, Lucchi F, Peccerillo A, Tranne A, Rossi PL, Frezzotti ML (2013) Stratigraphy and geological evolution of the Lipari volcanic complex (central Aeolian archipelago). Geol Soc London Mem 37:213-279

Frazzetta G, Gillot PY, La Volpe L, Sheridan MF (1984) Volcanic hazards of Fossa of Vulcano: data from the last 6,000 years. Bull Volcanol 47:105–124

Fulignati P, Gioncada A, Sbrana A (1998) Geologic model of the magmatic-hydrothermal system of Vulcano (Aeolian Islands, Italy). Mineral Petrol 62:195-222

Gallet Y, Genevey A, Le Goff M (2002). Three millennia of directional variation of the Earth's magnetic field in western Europe as revealed by archeological artefacts. Phys Earth Planet Int 131(1):81-89

Gamberi F (2001) Volcanic facies associations in a modern volcaniclastic apron (Lipari and Vulcano offshore, Aeolian Island Arc). Bull Volcanol 63(4):264-273

Gamberi F, Marani M, Savelli C (1997) Tectonic, volcanic and hydrothermal features of a submarine portion of the Aeolian arc (Tyrrhenian Sea). Marine Geology 140(1):167-181

Gambino S, Milluzzo V, Scaltrito A, Scarfì L (2012) Relocation and focal mechanisms of earthquakes in the south-central sector of the Aeolian Archipelago: New structural and volcanological insights. Tectonophysics, 524:108-115

Geyer A, Martì J (2014) The development of ring faults during collapse caldera formation. Frontiers in Earth Sciences. 2:22 doi:10.3389/feart.2014.00022

Gioncada A, Sbrana A (1991) La Fossa caldera, Vulcano: inferences from deep drillings. Acta Vulcanologica 1:115-125

Gioncada A, Mazzuoli R, Bisson M, Pareschi T (2003) Petrology of the post-40 ka products in the Vulcano-Lipari volcanic complex (Aeolian Islands, Italy): an example of volcanism controlled by tectonics. J Volcanol Geotherm Res 122:191-220

Gioncada A, Clocchiatti R, Sbrana A, Bottazzi P, Massare D, Ottolini L (1998) A study of melt inclusions at Vulcano (Aeolian islands, Italy): insights on the primitive magmas and on the volcanic feeding system. Bull Volcanol 60:286-306

Giordano G, De Benedetti A, Diana A, Diano G, Gaudioso F, Marasco F, Miceli M, Mollo S, Cas RAF, Funiciello R (2006) The Colli Albani mafic caldera (Roma, Italy): stratigraphy, structure and petrology. J Volcanol Geotherm Res 155(1): 49-80

Grosse P, van Wyk de Vries B, Petrinovic IA, Euillades PA, Alvarado G (2009) Morphometry and evolution of arc volcanoes. Geology 37:651–654

Grosse P, van Wyk de Vries B, Euillades PA, Kervyn M, Petrinovic IA (2011) Systematic morphometric characterization of volcanic edifices using digital elevation models. Geomorphology 136:114–131

Gudmundsson A (2011) Deflection of dykes into sills at discontinuities and magma-chamber formation. Tectonophysics 500:50-64

Gurioli L, Zanella E, Gioncada A, Sbrana A (2012) The historic magmatic-hydrothermal eruption of the Breccia di Commenda, Vulcano, Italy. Bull Volcanol 74:1235–1254 doi:10.1007/s00445-012-0590-4

Hobden BJ, Houghton BF, Nairn IA (2002) Growth of a young, frequently active composite cone: Ngauruhoe Volcano, New Zealand. Bull Volc 64:392–409

Ihinger PD, Hervig RL, McMillan PF (1994) Analytical methods for volatiles in glasses. Rev Mineral Geochem 30:67–121

Intrieri E, Di Traglia F, Del Ventisette C, Gigli G, Mugnai F, Luzi G, and Casagli N (2013) Flank instability of Stromboli volcano (Aeolian Islands, Southern Italy): integration of GB-InSAR and geomorphological observations: Geomorphology 201:60.69 doi:10.1016/j.geomorph.2013.06.007.

Keller J (1970) Die historischen eruptionen von Vulcano und Lipari. Z deutsch Geol Ges 121:179–185

Keller J (1980) The island of Vulcano. Rend SIMP 36:369–414

Kratzmann DJ, Carey S, Scasso R, and Naranjo JA (2009) Compositional variations and magma mixing in the 1991 eruptions of Hudson volcano, Chile: Bull Volcanol 71:419–439, doi: 10.1007/s00445-008-0234-x.

Lange R L, Carmichael I S (1990) Thermodynamic properties of silicate liquids with emphasis on density, thermal expansion and compressibility. Rev Mineral Geochem 24:25-64

Lanza R, Zanella E. (2003). Paleomagnetic secular variation at Vulcano (Aeolian Islands) during the last 135 kyr. Earth Planet Sci Lett 213(3):321-336.

Le Voyer M, Asimow P D, Mosenfelder J L, Guan Y, Wallace P J, Schiano P et al (2014) Zonation of H_2O and F Concentrations around Melt Inclusions in Olivines. J Petrol 55:685-707

Lloyd AS, Plank T, Ruprecht P, Hauri EH, Rose W (2013) Volatile loss from melt inclusions in pyroclasts of differing sizes. Contrib Mineral Petrol 165:129-153

Lowestern JB (1994) Chlorine, fluid immiscibility, and degassing in peralkaline magmas from Pantelleria, Italy. Am Mineral 79:353–369

Luhr J F (2001) Glass inclusions and melt volatile contents at Paricutin Volcano, Mexico. Contrib Mineral Petrol 142:261-283

Manville V, Németh K, Kano K (2009) Source to sink: a review of three decades of progress in the understanding of volcaniclastic processes, deposits, and hazards. Sedim Geol 220:136-161

Mercalli G, Silvestri O (1891) Le eruzioni dell'isola di Vulcano, incominciate il 3 Augusto 1888 e terminate il 22 Marzo 1880, Ann Uff Centr Meteorol Geodin 10(4): 1-213

Métrich N, Wallace P (2008) Volatile abundance in basaltic magmas and their degassing paths tracked by melt inclusions. In: Putirka, K. D. & Tepley, F. J., III (eds) Minerals, Inclusions and Volcanic Processes. Mineralogical Society of America and Geochemical Society, Rev Mineral Geochem 69:363-402

Moore G, Vennemann T, Carmichael I S E (1998) An empirical model for the solubility of H2O in magmas to 3 kilobars. Am Mineral 83:36-42

Nakamoto K (1978) Infrared and Raman spectra of inorganic and coordination compounds. John Wiley & Sons, Ltd.

Palladino, D. M., Simei, S., Sottili, G., & Trigila, R. (2010). Integrated approach for the reconstruction of stratigraphy and geology of Quaternary volcanic terrains: an application to the Vulsini Volcanoes (central Italy). Geol Soc Am Special Papers 464:63-84

Parfitt EA (2004) A discussion of the mechanisms of explosive basaltic eruptions. J Volcanol Geotherm Res 134:77–107.

Peccerillo A, Taylor S R (1976) Geochemistry of Eocene calc-alkaline volcanic rocks from the Kastamonu area, northern Turkey. Contrib Mineral Petrol 58:63-81

Peccerillo A, Frezzotti ML, De Astis G, Ventura G (2006) Modeling the magma plumbing system of Vulcano Aeolian Islands, Italy by integrated fluid inclusion geo-barometry, petrology and geophysics. Geology 34:17–20

Petronis MS, Delcamp A, de Vries BVW (2013) Magma emplacement into the Lemptégy scoria cone (Chaîne Des Puys, France) explored with structural, anisotropy of magnetic susceptibility, and Paleomagnetic data. Bull Volcanol 75(10):1-22

Pinel V, Jaupart C (2004) Magma storage and horizontal dyke injection beneath a volcanic edifice. Earth Planet Sci Lett 221:245-262

Pistolesi M, Rosi M, Cioni R, Cashman KV, Rossotti A, Aguilera E (2011) Physical volcanology of the post-twelfth-century activity at Cotopaxi volcano, Ecuador: Behavior of an andesitic central volcano. Geol Soc Am Bull 123(5-6):1193–1215, doi:10.1130/B30301.1.

Principe C, Tanguy J C, Arrighi S, Paiotti A, Le Goff M, Zoppi U (2004) Chronology of Vesuvius' activity from AD 79 to 1631 based on archeomagnetism of lavas and historical sources, Bull Volcanol 66: 703–724

Rodriguez-Gonzalez A, Fernandez-Turiel J L, Perez-Torrado F J, Gimeno D, Aulinas M (2010) Geomorphological reconstruction and morphometric modelling applied to past volcanism. Int J Earth Sci 99:645-660

Roedder E (1984) Fluid inclusions. Rev Mineral 12:1–646

Roeder P L, Emslie R (1970) Olivine-liquid equilibrium. Contrib Mineral Petrol 29:275-289

Roggensack K, Williams S N, Schaefer S J, Parnell R A (1996) Volatiles from the 1994 eruptions of Rabaul: understanding large caldera systems. Science 273:490-493

Romagnoli C, Casalbore D, Bosman A, Braga R, Chiocci F L (2013) Submarine structure of Vulcano volcano (Aeolian Islands) revealed by high-resolution bathymetry and seismo-acoustic data. Marine Geology 338:30-45.

Rubin AM (1995) Propagation of magma-filled cracks. Annu Rev Earth Planet Sci 23:287–336

Saunders S J (2001) The shallow plumbing system of Rabaul caldera: a partially intruded ring fault?. Bull Volcanol 63:406-420

Scandone R, Cashman KV, Malone S D (2007) Magma supply, magma ascent and the style of volcanic eruptions. Earth Planet Sci Lett 253:513-529

Sigmundsson F, Hreinsdóttir S, Hooper A, Árnadóttir T, Pedersen R, Roberts MJ, Oskarsson N, Auriac A, Decriem J, Einarsson P, Geirsson H, Hensch M, Ofeigsson BG, Sturkell E, Sveinbjornsson H, Feigl KL (2010). Intrusion triggering of the 2010 Eyjafjallajokull explosive eruption. Nature 468(7322):426-430

Stolper E (1982) The speciation of water in silicate melts. Geochim Cosmochim Acta 46:2609-2620

Tanguy JC, Le Goff, M, Principe C, Arrighi S, Chillemi V, Paiotti A, La Delfa S Patanè G (2003) Archeomagnetic dating of Mediterranean volcanics of the last 2100 years: validity and limits. Earth Planet Sci Lett 211(1):111-124

Tait S (1992) Selective preservation of melt inclusions in igneous phenocrysts. Am Mineral 77:146-155

Takada A (1999) Variations in magma supply and magma partitioning: the role of tectonic settings. J Volcanol Geotherm Res 93(1):93-110

Tarasewicz J, White RS, Woods AW, Brandsdóttir B and Gudmundsson MT (2012) Magma mobilization by downward-propagating decompression of the Eyjafjallajökull volcanic plumbing system. Geoph Res Lett 3919:1-5 doi: 10.1029/2012GL053518.

Tibaldi A. (2010) A new geological map of Stromboli volcano (Tyrrhenian Sea, Italy) based on application of lithostratigraphic and unconformity-bounded stratigraphic (UBS) units. Geol Soc Am Special Papers 464:33-49

Ventura G, Vilardo G, Milano G, Pino NA (1999) Relationships among crustal structure, volcanism and strike-slip tectonics in the Lipari-Vulcano volcanic complex Aeolian Islands, Southern Tyrrhenian Sea, Italy. Phys Earth Planet Int 116:31–52

Vetere F, Behrens H, Misiti V, Ventura G, Holtz F, De Rosa R, Deubener J (2007) The viscosity of shoshonitic melts (Vulcanello Peninsula, Aeolian Islands, Italy): insight on the magma ascent in dikes. Chem Geol 245:89-102

Voltaggio M, Branca M, Tuccimei P, Tecce F (1995) Leaching procedure used in dating young potassic volcanic rocks by the 226Ra/230Th method. Earth Planet Sci Lett 136:123–131

Wallace P J, Carmichael I S (1994) Petrology of Volcán Tequila, Jalisco, Mexico: disequilibrium phenocryst assemblages and evolution of the subvolcanic magma system. Contrib Mineral Petrol 117: 345-361

Walter T R, Troll V R (2001) Formation of caldera periphery faults: an experimental study. Bull Volcanol 63(2-3):191-203

Watson E B (1994) Diffusion in volatile-bearing magmas. In: Carroll, M. & Holloway, J. R. (eds) Volatiles in Magmas. Mineralogical Society of America, Rev Mineral Geochem 30:371-411

Wysoczanski RJ, Tani K (2006) Spectroscopic FTIR imaging of water species in silicic volcanic glasses and melt inclusions: an example from the Izu-Bonin arc. J Volcanol Geotherm Res 156:302–314

Zanon V, Frezzotti M L, Peccerillo A (2003) Magmatic feeding system and crustal magma accumulation beneath Vulcano Island (Italy): evidence from CO_2 fluid inclusions in quartz xenoliths. J Geophys Res: Solid Earth (1978–2012) 108(B6)

Tables captions

Table 1. Synthesis of the direct and indirect (i.e. based on the exotic rhyolitic tephra of Pilato and Rocche Rosse eruptions at Lipari) geochronological constraints for the age of Vulcanello eruptions.

Table 2. Synoptic table comparing the stratigraphic reconstruction proposed in this work for Vulcanello, using lithosomes and eruptive units, with the previous reconstructions by Keller (1980), De Astis et al. (2013), Di Traglia et al. (2013).

Table 3. Main eruptive units of the Vulcanello lithosomes with related sedimentological features.

Table 4. DEM-derived calculations of the Vulcanello lavas and tephras erupted volumes.

Table 5. Whole Rock Composition (XRF, wt%) and CIPW norm calculation of Vulcanello samples selected for the MI study. All samples are juvenile lapilli.

Table 6. Major element and volatile compositions measured on melt inclusions (above) and recalculated compositions (below, see text for recalculation details). Data in wt%. Each major element analysis is the mean of several analyses on the same MI (see Methods in Supplementary material). Total iron as FeO_T. Mg# is $Mg^{2+}/(Mg^{2+}+ Fe^{2+})$, assuming that 80% of the total iron is present as Fe^{2+}. P is the vapor saturation pressure in Pascal calculated following Moore et al. (1998).

Table 7. Major element compositions and volatile content of glass of the submarine lava from Vulcanello 2 activity. Each major element analysis is the mean of several analyses on the same

fragment. Total iron is reported as FeO_T. All analyses are in wt%. Mg# and P are defined as in Table 5.

Figure captions

Figure 1. a) The island of Vulcano; b) Geology of Vulcano modified after Di Traglia et al. (2013); c) Vulcanello peninsula (view from La Fossa).

Figure 2. a) Geology of Vulcanello peninsula from the new geological survey at 1:10,000 scale; b) cross section along the line A-B.

Figure 3. Representative stratigraphic log of the whole Vulcanello eruptive activity (not to scale). Colors of the volcano-stratigraphic units as in Figure 2.

Figure 4. Stratigraphic relationships between Vulcanello, La Fossa and Pilato (Lipari) deposits on the Vulcanello platform. Logs 26 and 3 are from natural sections while logs 31, 30, 29, 34 and 6 are from machine-excavated and hand-dug pit trenches. The colors of the units correlations refer to Figure 2 and 3 unit colors.

Figure 5. Outcrops of Vulcanello 1 Lithosome; a) Lava platform (Vulcanello 1A Eruptive Unit, facies Plateau Lava; b) the two different facies in Vulcanello 1A Eruptive Unit, the Plateau Lava and the Grey Pyroclastics; dyke of Vulcanello 2 that cuts the entire stratigraphic sequence of Vulcanello 1 activity (outcrop n. 27 in Fig. 2) ; c) Vulcanello 1 Lithosome stratigraphic sequence (outcrop n. 26 in Fig. 2a);

Figure 6. a) Stratigraphic contact between Vulcanello 2 Lithosome (Vulcanello 2 Eruptive Unit) and Vulcanello 1 Lithosome (Vulcanello 1D Eruptive Unit) separated by reworked material on Vulcanello S-SE slope; b) stratigraphic relationship between Vulcanello 2 Lithosome (Vulcanello 2 Eruptive Unit) and the Pal B rhyolitic layer from La Fossa activity on the northeast cliff of Vulcanello platform (outcrop n. 26 Fig. 2a).

Figure 7. Stratigraphic relationships between Vulcanello 1 Lithosome and Pal B rhyolitic layer from La Fossa activity on the southwest cliff of Vulcanello platform (outcrop n. 2 in Fig. 2a).

Figure 8. a) Stratigraphic relationships between Pal B rhyolitic layer from La Fossa activity and Rocche Rosse tephra from the Mt. Pilato (Island of Lipari) activity on the Vulcanello platform (machine-excavated trench, site n. 31 Fig. 2a); b) Stratigraphic relationships between the distal Rocche Rosse tephra from the Mt. Pilato and Commenda tephra from La Fossa activity and the Vulcanello 3 Lithosome (machine-excavated trench, site n. 29 Fig. 2). The paleosol marks the time interval between the first eruptive cluster, preceding the Commenda and the Rocche Rosse activity, and the second cluster, represented by the Vulcanello 3 activity.

Figure 9. a) Stratigraphic contacts between ash-fall deposits (Vulcanello 3C and 3E Eruptive Units) from phreatic eruptions and lava flow deposit (Vulcanello 3B Eruptive Unit) of Vulcanello 3 Lithosome (outcrop n. 11 in Fig. 2a); b) Vulcanello 3 Lithosome Vulcanello 3D Eruptive Unit. c)-d) Details of the Vulcanello 3C and 3E Eruptive Units, respectively. e) Tephra deposits on the Vulcanello platform (Vulcanello 1A) as found in hand-dug trench (site n. 34 in Fig. 2a), showing Vulcanello 3A, 3C and 3E overlying the Commenda distal tephra.

Figure 10. K_2O vs SiO_2 wt% diagram (Peccerillo and Taylor 1976) of the Vulcanello samples studied in this work (bulk rock analysis, squares) compared with Vulcanello and La Fossa bulk rock composition (gray field) from Davì et al. (2009) and De Astis et al. (2013).

Figure 11. Microphotographs of melt inclusions in olivine after sectioning for infrared spectroscopy. a) Wrinkled texture in fully enclosed melt inclusion in Vulcanello 1C Eruptive Unit; b) glassy texture in fully enclosed melt inclusions in Vulcanello 2 Eruptive Unit; c) Main morphological features of MI in the selected samples (presence of vapor bubbles, texture).

Figure 12. Major element variation diagrams for Vulcanello melt inclusions (MI), glass of the pillow lavas (V2p glass), and whole rock (WR) samples. In the K_2O vs SiO_2 plot, fields for MI composition of the Fossa products (dotted line) and for Vulcanello 1 products (full line) after Gioncada et al. (1998) are reported. The stars indicate the parent basaltic composition of the Vulcanello magmas (Davì et al., 2009) found in MI in Fo90 olivine (Gioncada et al. 1998). For

comparison to the whole rocks, the MI composition is plotted after normalization of major elements to 100.

Figure 13. Schematic reconstruction of the Vulcanello feeding system. The presence of a magmatic chamber below the La Fossa cone is required by the diffuse degassing registered in the area and is suggested by the high geothermal gradients measured in the Agip boreholes (VP1 and IV1), pointing to magmatic temperatures at 2000-3000 m of depth. The depth of magma storage is based on different lines of evidence: i) geophysical constraints for the lithological boundaries at depth (Chiarabba et al. 2004; Gambino et al. 2012); ii) pressure from fluid inclusions in quartz-bearing xenoliths (Zanon et al. 2003); iii) minimum pressure of crystallization from volatile content of melt inclusions in phenocrysts (Clocchiatti et al. 1994; Gioncada et al. 1998). These different approaches agree in indicating a polibaric plumbing system along the entire Vulcano history, with magma storage at about 20 km of depth, 13-8 km, 5-3 km and a shallow storage zone at 1-2 km beneath the La Fossa cone (Peccerillo et al. 2006) and Vulcanello (this work). The short-lived very shallow storage region involved in Vulcanello activity was fed probably at the onset of Vulcanello 1 phase

Figure_1
Click here to download Figure: Figure 1.jpg

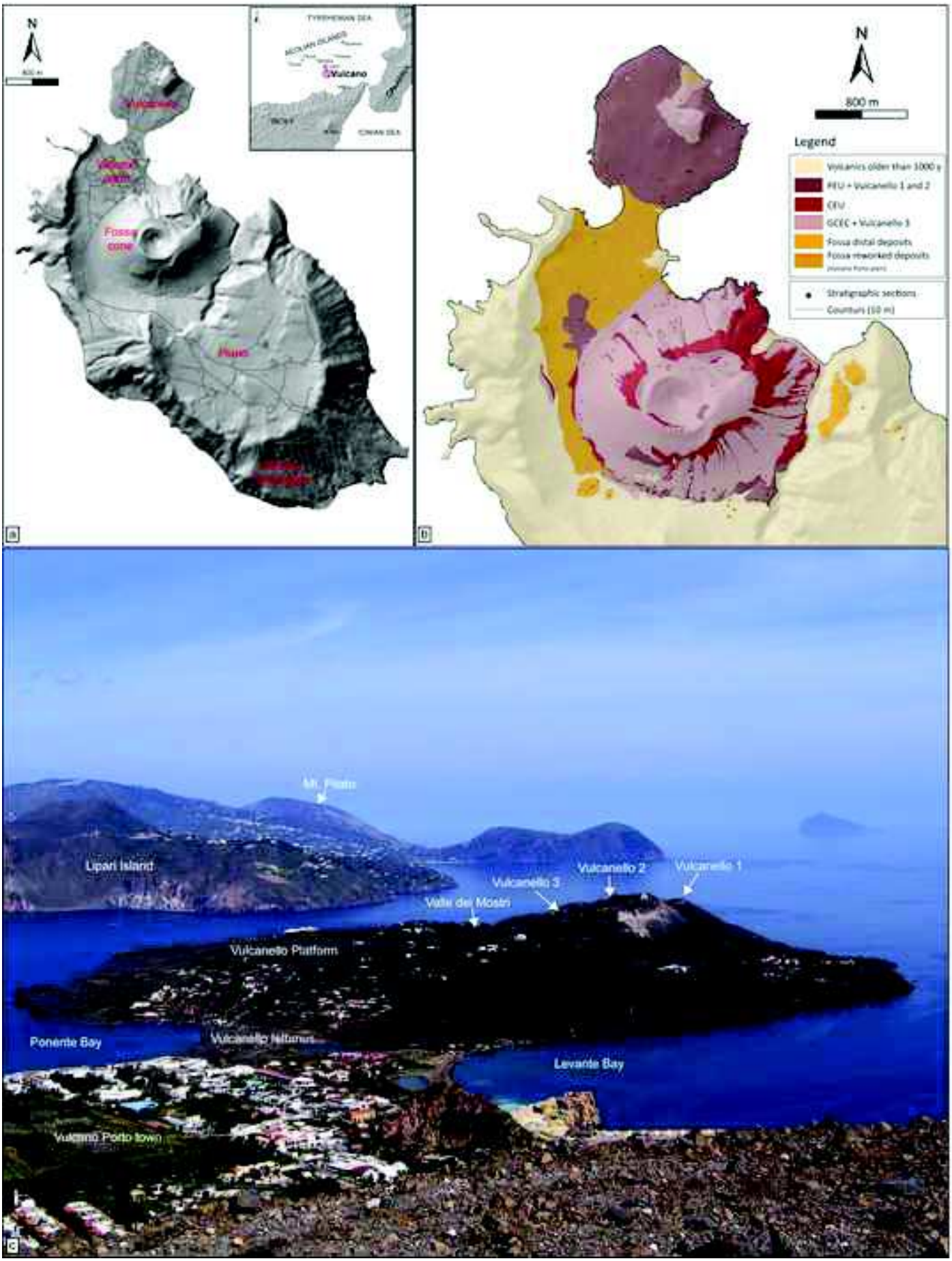

Figure_2
Click here to download Figure: Figure 2.jpg

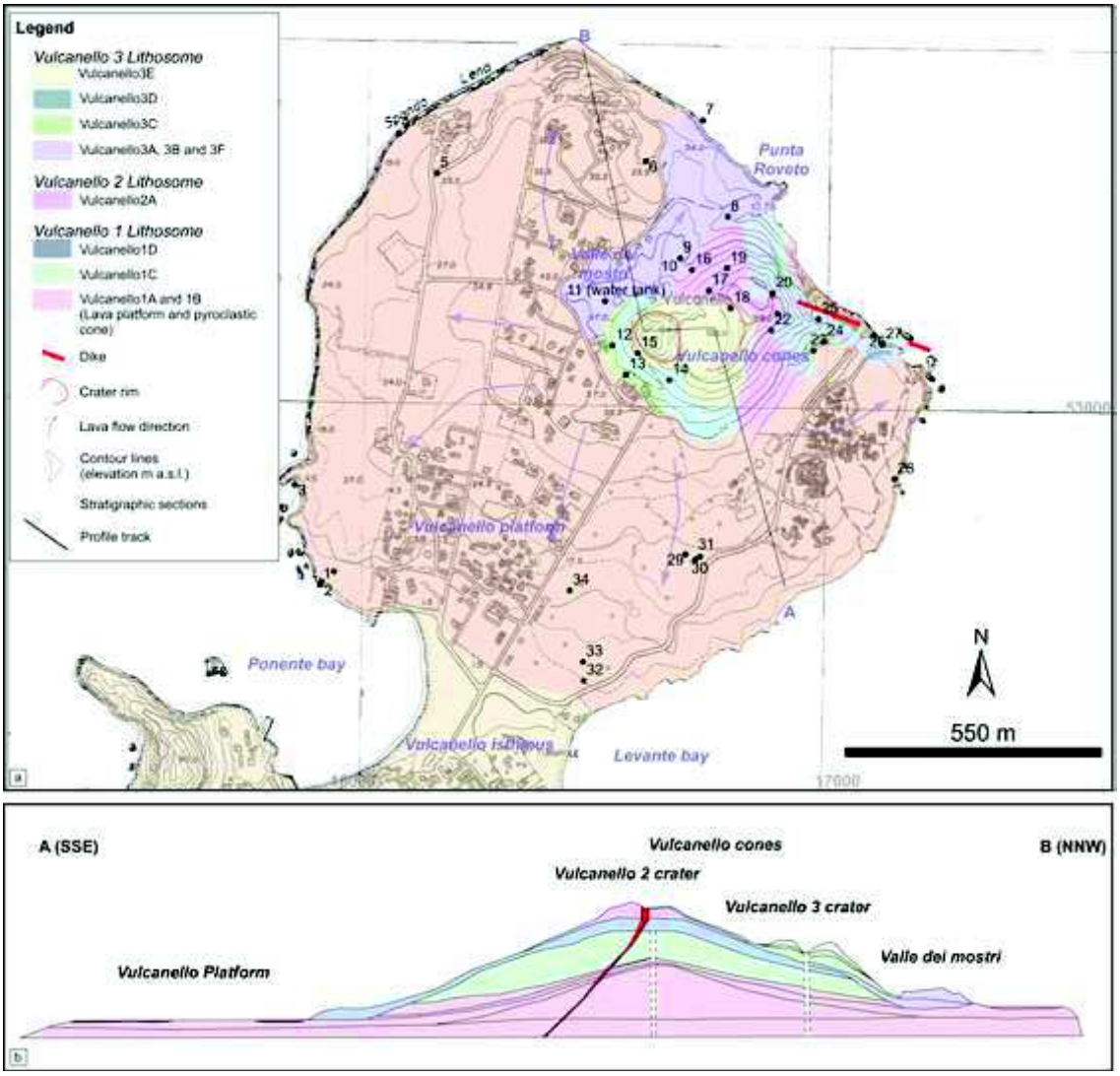

Figure_3
Click here to download Figure: Figure 3.jpg

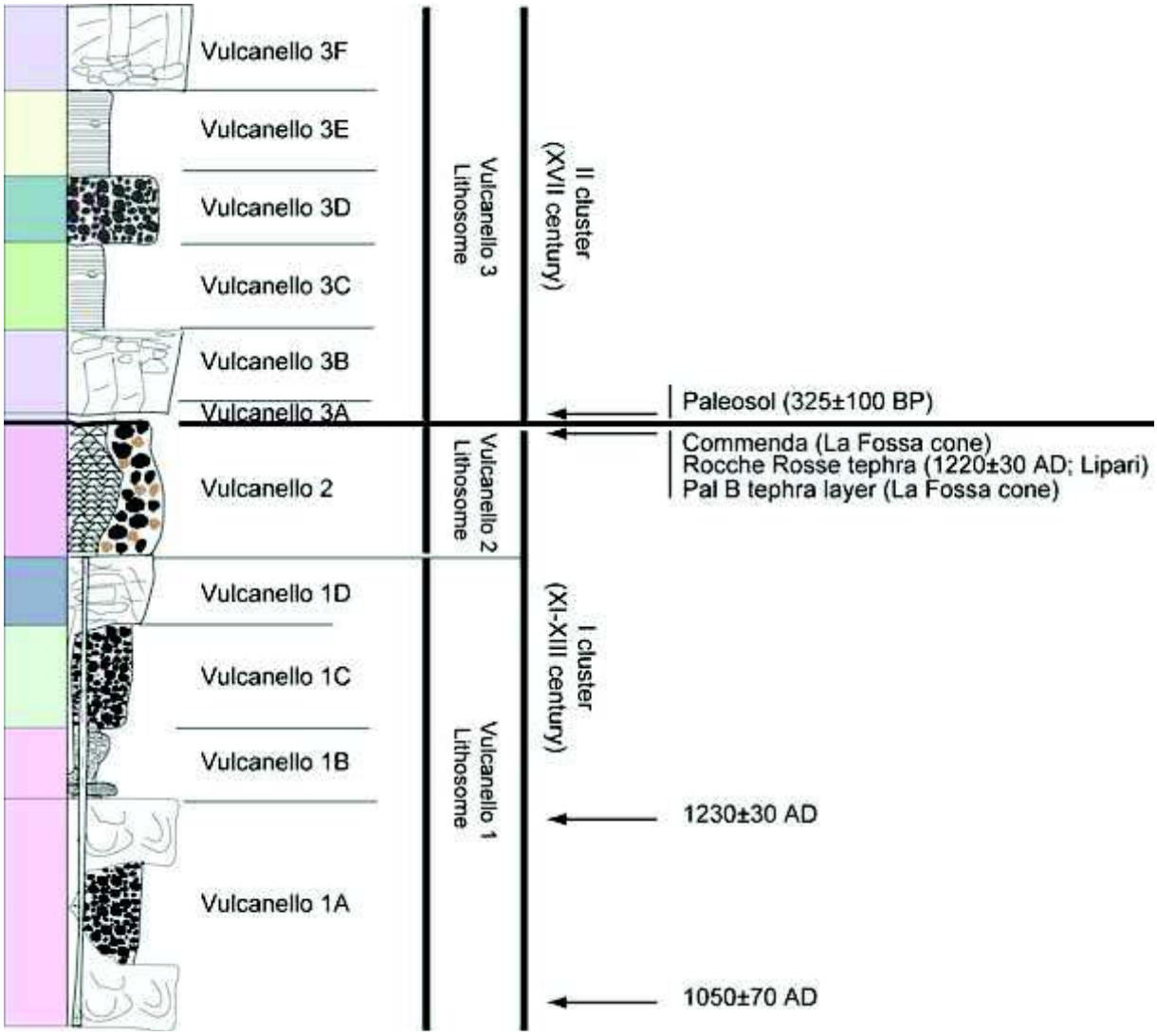

Figure_4
Click here to download Figure: Figure 4.jpg

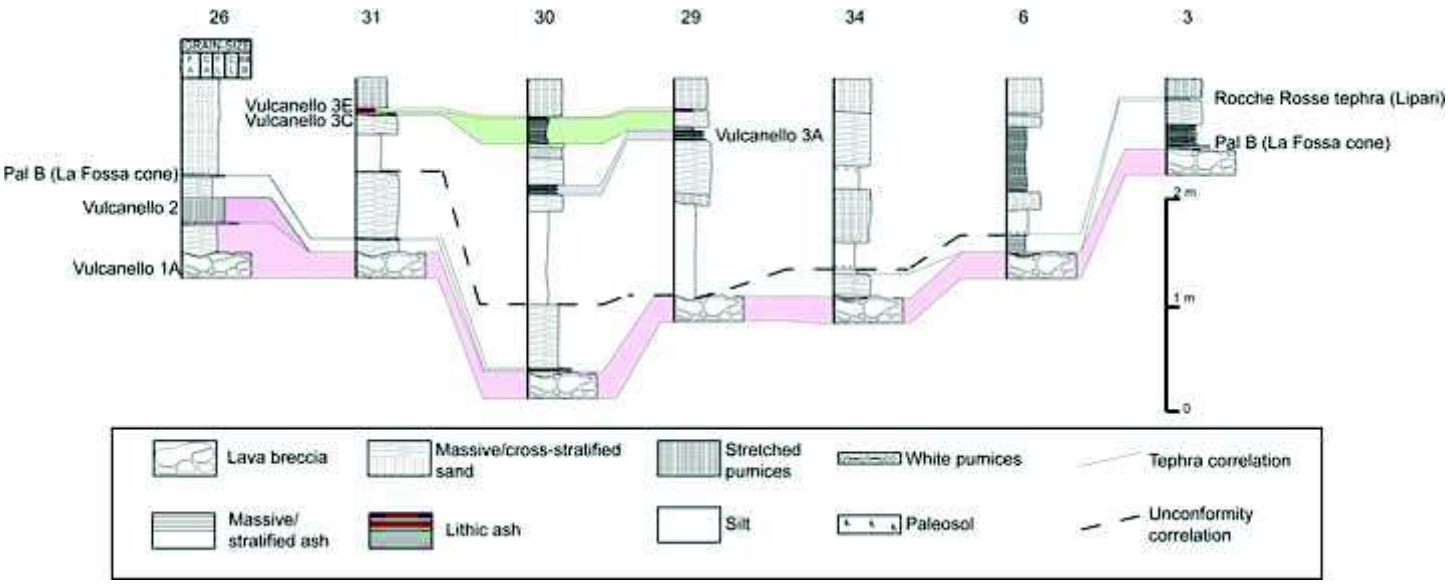

Figure_5
Click here to download Figure: Figure 5.jpg

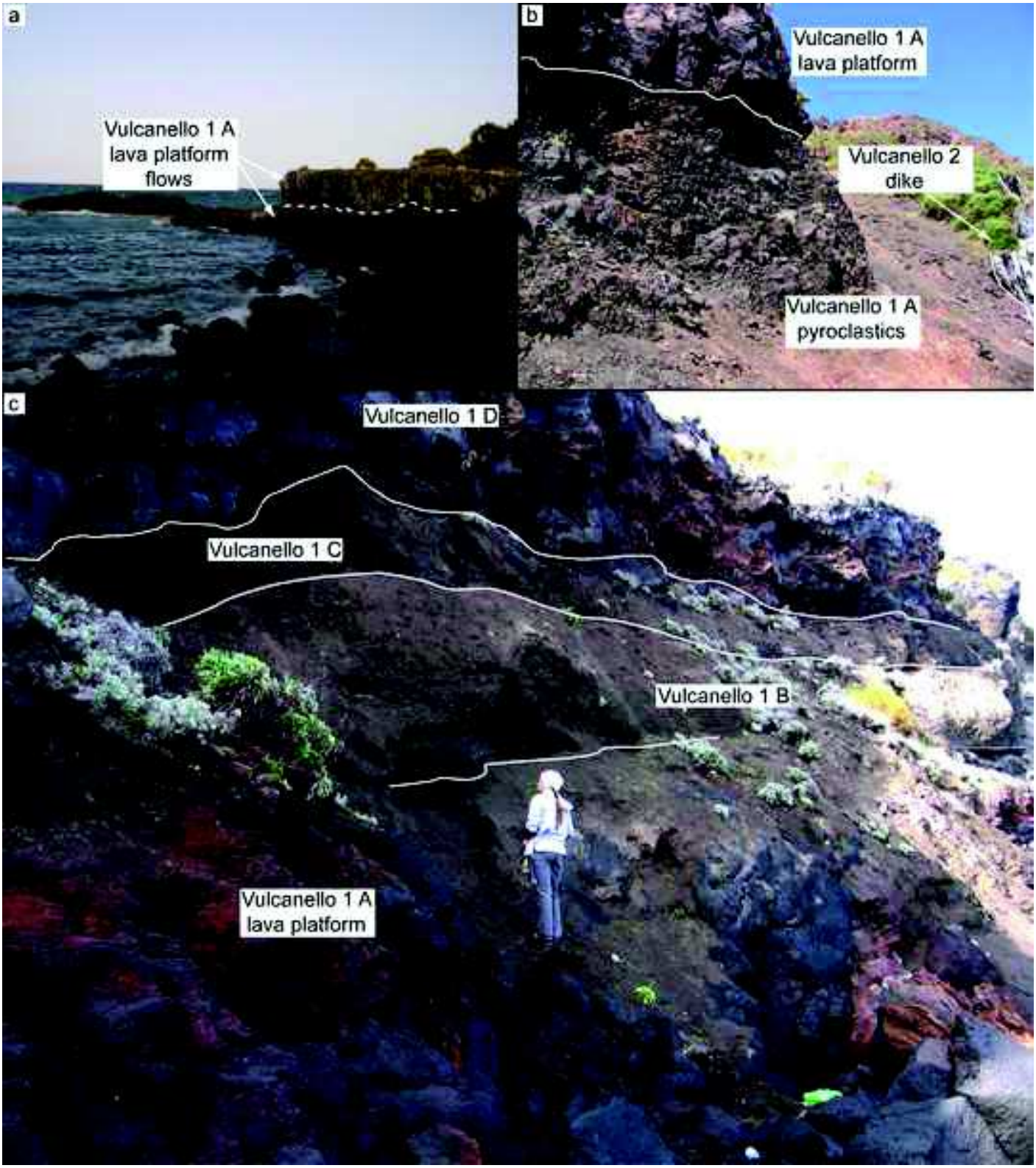

Figure_6
Click here to download Figure: Figure 6.jpg

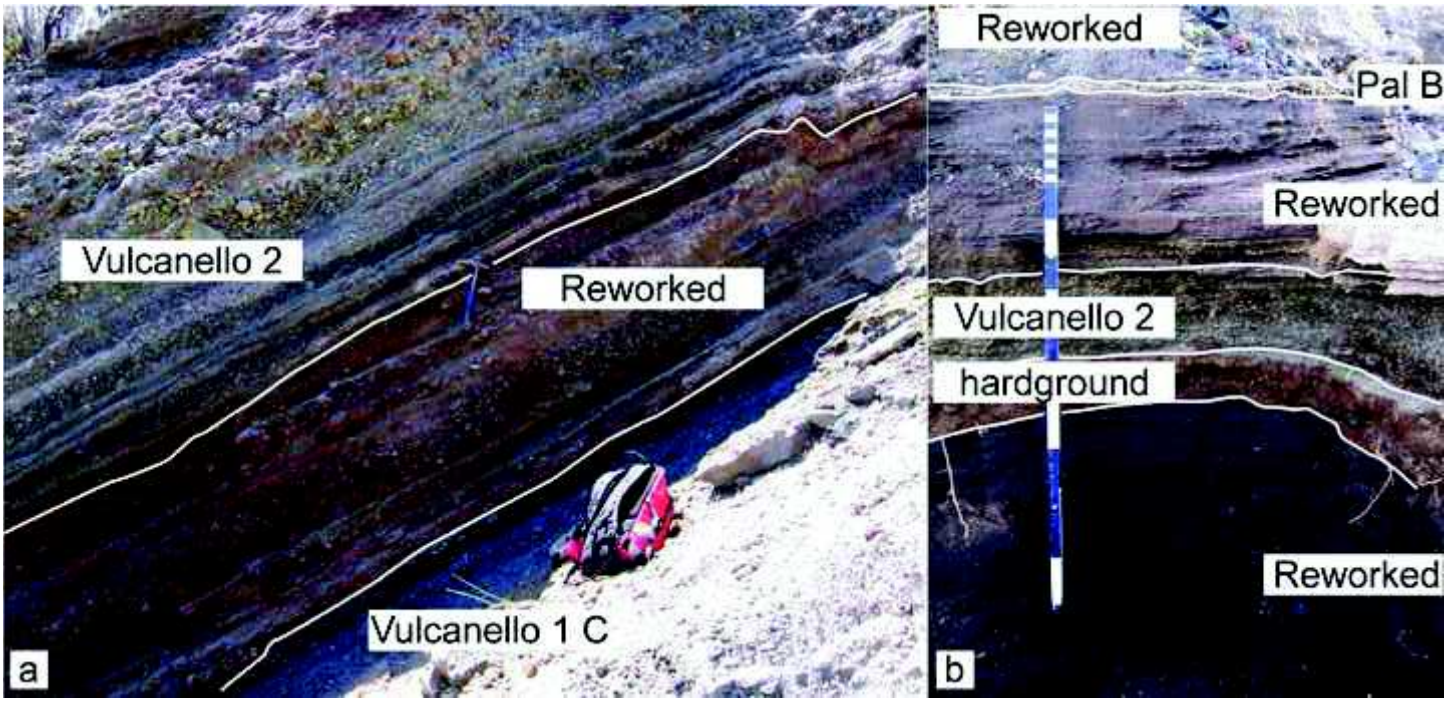

Figure_7
Click here to download Figure: Figure 7.jpg

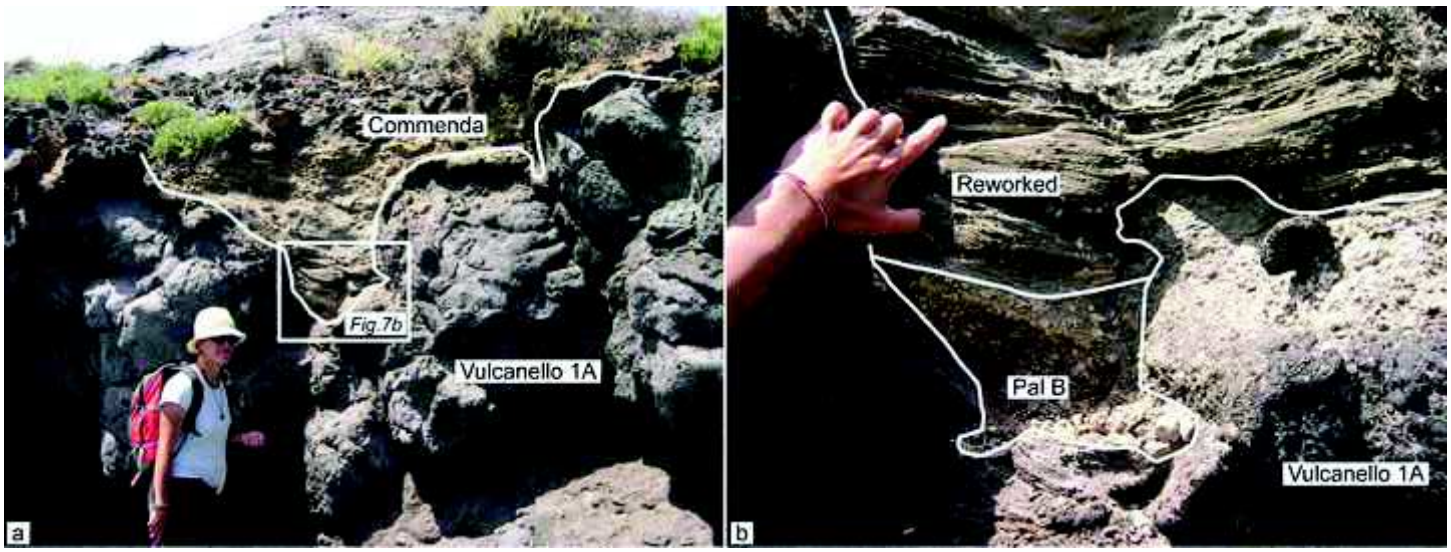

Figure_8
Click here to download Figure: Figure 8.jpg

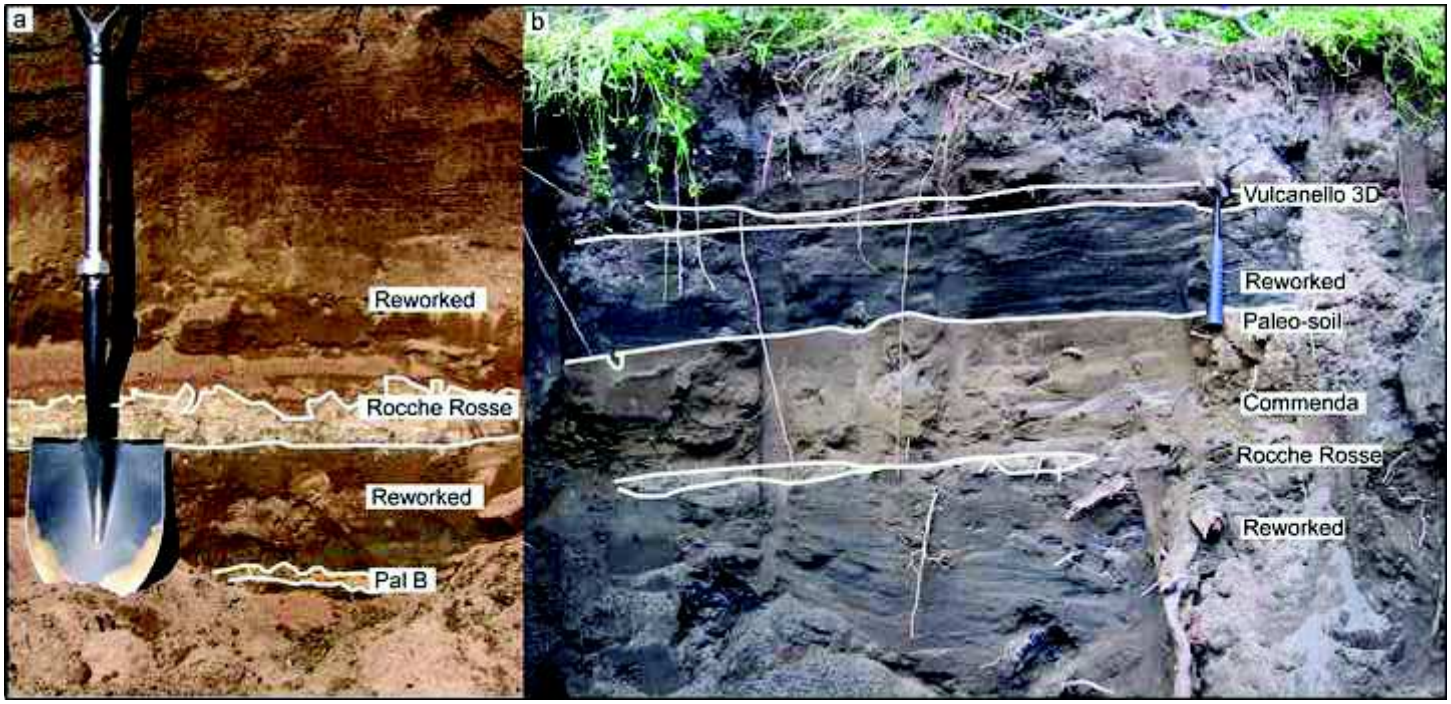

Figure_9
Click here to download Figure: Figure 9.jpg

Figure_10
Click here to download Figure: Figure_10.JPG

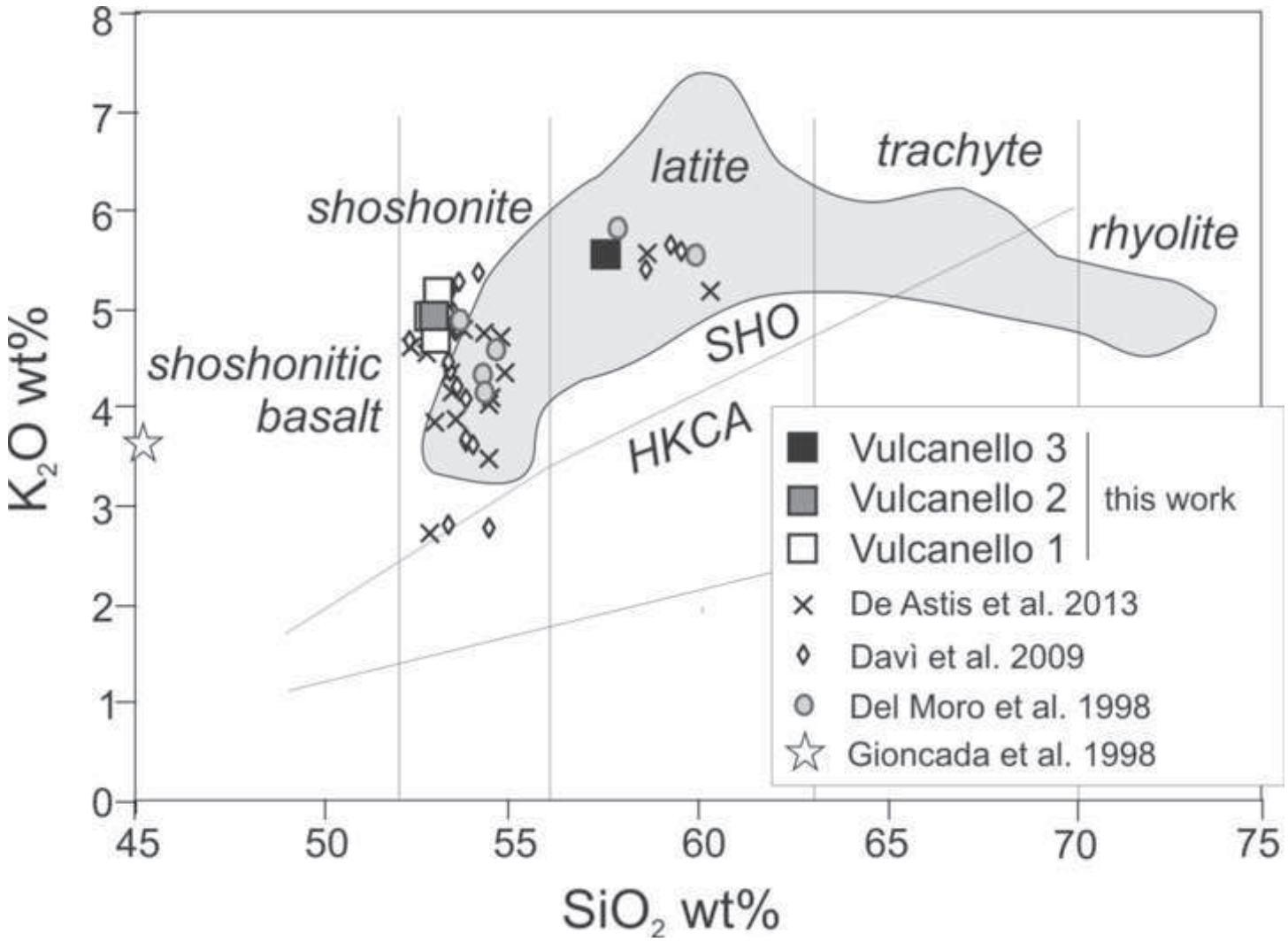

Figure_11
Click here to download Figure: Figure 11.jpg

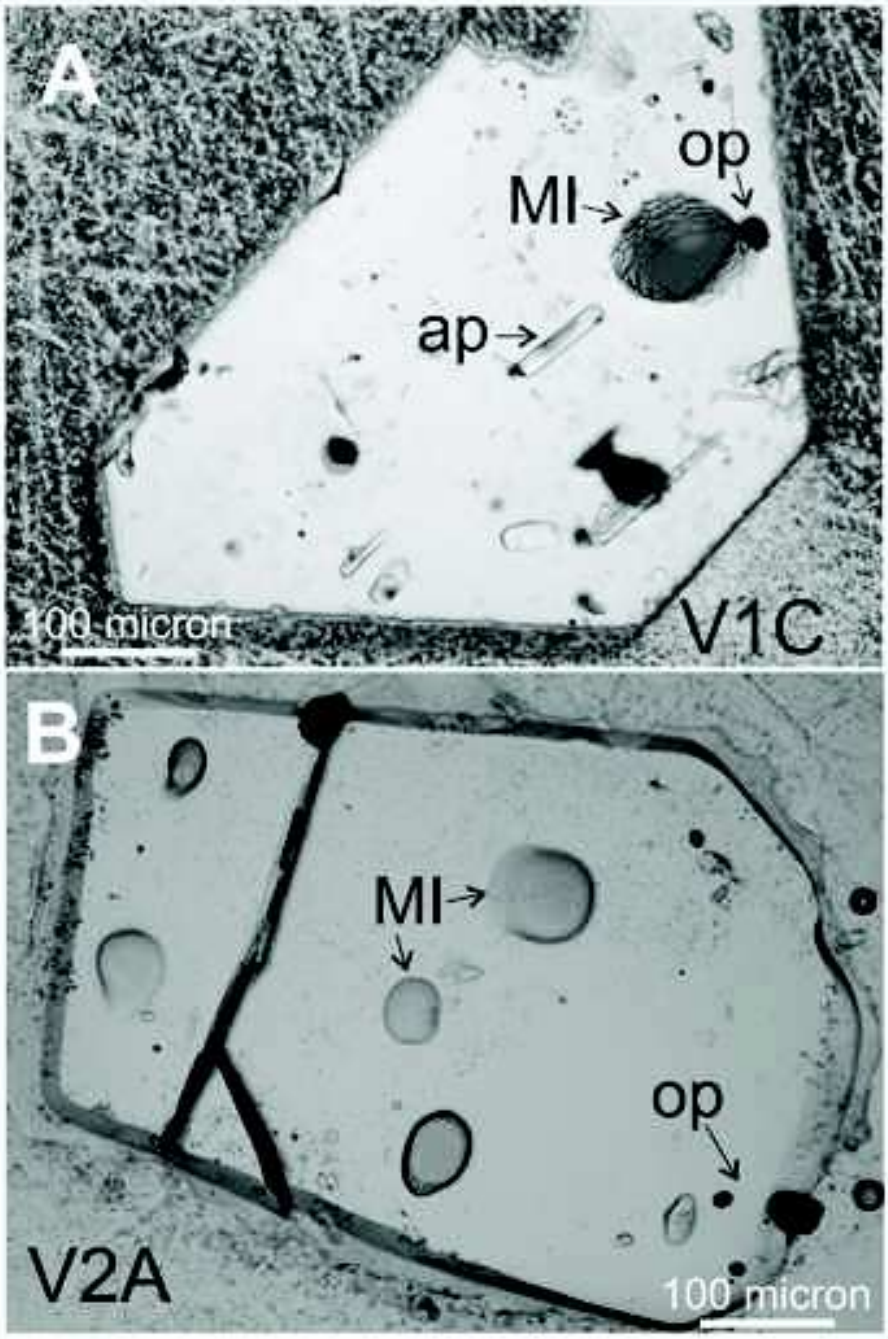

C

Sample	Vaporbubbles	Texture
V1A	?	finely crystalline
V1B	none	glassy
V1C type 1	none	glassy
V1C type 2	none	glassy, wrinkled
V2A	none	glassy
V3D	none	glassy

Figure_12
Click here to download Figure: Figure_12.JPG

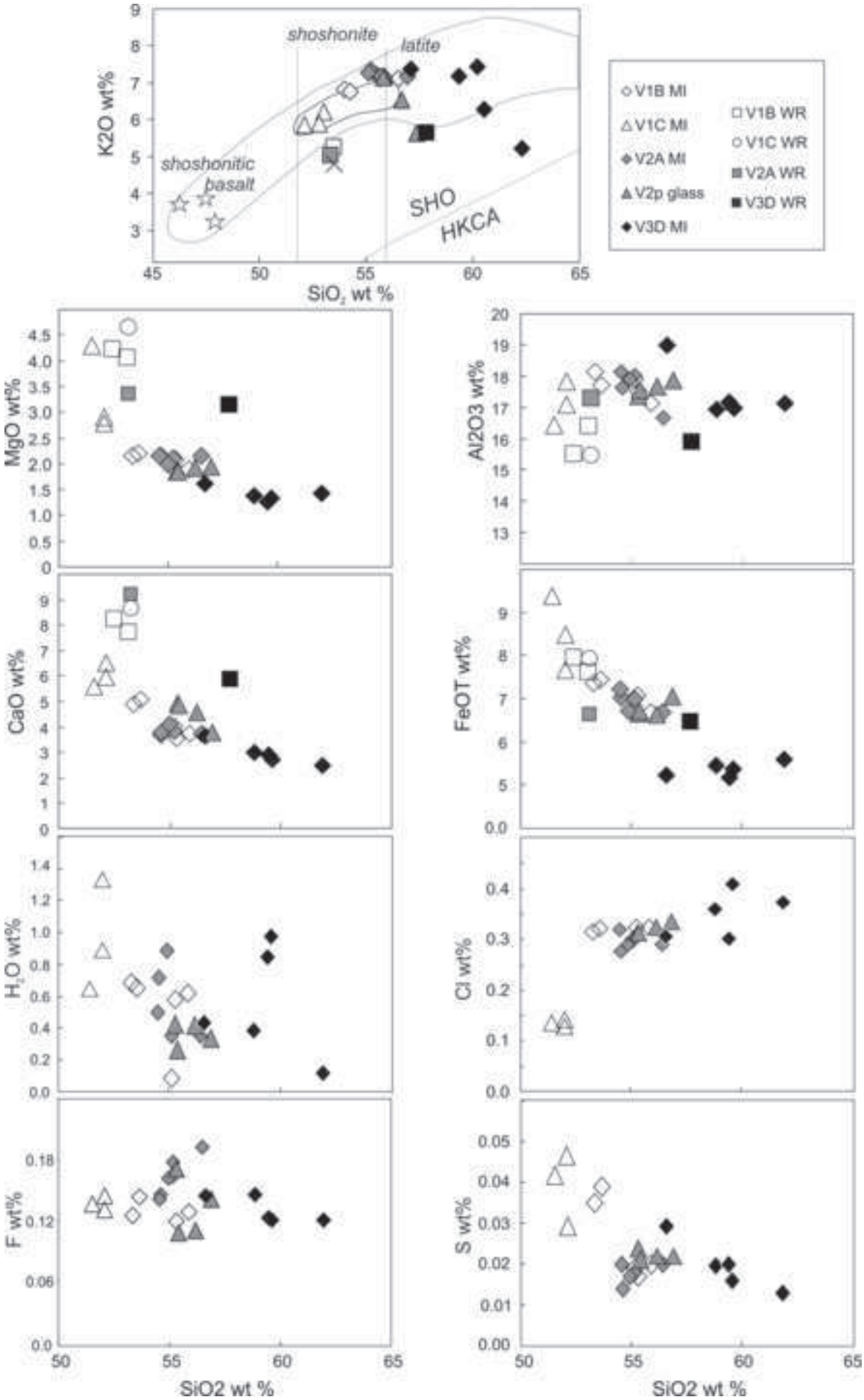

Figure_13
Click here to download Figure: Figure 13.JPG

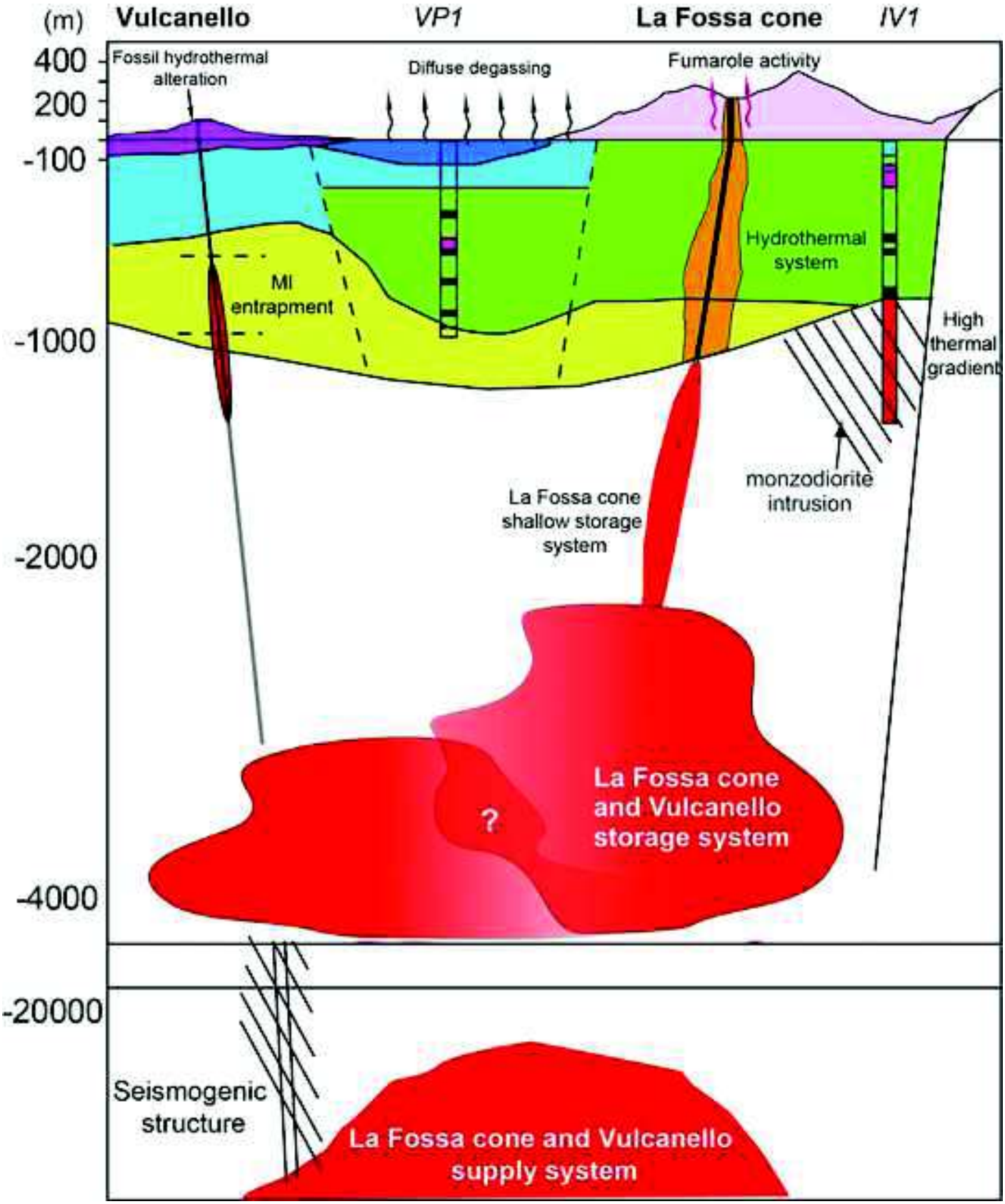

Table_1

	Pilato tephra	Vulcanello platform	Rocche Rosse tephra	Vulcanello 3
Mercalli and Silvestri (1891) historical records		183-126-91 BC, early emersion		
De Fiore (1922) historical records		183-126-91 BC		
Keller (1970), ^{14}C dating	1220±100 BP, paleosol	183-126-91 BC		325±100 year BP, paleosol
Keller (1980)		183-126-91 BC		
Voltaggio et al. (1995) $^{226}Ra/^{230}Th$ dating		1.9±0.2 ky		
Keller (2002), ^{14}C dating	AD 776 (+110/−90)			
Tanguy et al. (2003) archeomagnetic data			AD 1220 ± 30 (Rocche Rosse lava)	
Lanza and Zanella (2003) paleomagnetic data		1.9 ± 0.1 ka		
Arrighi et al. (2006) archeomagnetic data [based on secular variation of the geomagnetic field reconstructed from Italian Lavas;Tanguy et al., 2003]		AD 1180 ± 30 AD 1050 ± 70 AD 1080 ± 50 AD 1000 ± 60 AD 1180 ± 70 AD 1230 ± 30 AD 1100 ± 60		
Caron et al. (2012) ^{14}C dating			0.61±0.02 cal ka BP (criptotephra in deep-sea core)	
Gurioli et al. (2012) archeomagnetic data [based on French Secular Variation curve;Gallet et al. 2002]			AD 918–1302 (Breccia di Commenda lithic clasts)	

Table_2

Keller (1980)	**De Astis et al. (2006, 2013)**	**Di Traglia et al. (2013a)**	**This work**	
Structural Units	*Formations*	*Units*	*Lithosome*	*Units*
Vulcanello 3	Vulcanello 3b (pyroclastics)	Vulcanello 3 (comprising Roveto lava flow)	Vulcanello 3	Vulcanello 3F (Valle dei Mostri Lava Flow)
				Vulcanello 3E
				Vulcanello 3D
Roveto lava flow	Vulcanello 3a (Roveto lava flow)			Vulcanello 3C
				Vulcanello 3B (Roveto Lava Flow)
				Vulcanello 3A
Lava platform	Vulcanello 2	Vulcanello 2	Vulcanello 2	Vulcanello 2
Vulcanello 2	Vulcanello 1b (Lava platform)	Vulcanello 1 (comprising lava platform)	Vulcanello 1	Vulcanello 1D
				Vulcanello 1C
				Vulcanello 1B
Vulcanello 1	Vulcanello 1a (pyroclastics)			Vulcanello 1A (Lava platform and pyroclastic cone)

Table_3

Eruptive Units	Bedding	Texture and grading	Clast size	Clast shape	Clast vesicularity	Welding	Lithic fragments
Vulcanello 1 Lithosome							
Vulcanello 1A (Lava)	Planar to lenticular; pahoehoe morphology	Massive	–	–	–	–	–
Vulcanello 1A (grey pyroclastics)	Planar	Massive	Fine to coarse lapilli; sporadic bombs	Irregular to elongated clasts	Moderate to high vesicularity	No welding	Lava
Vulcanello 1B	Planar	Massive (base), normally to reversely graded	Ash to lapilli; sporadic bombs	Irregular	High vesicularity	No welding	Lava
Vulcanello 1C	Stratified	Normally graded	Lapilli to bombs	Irregular	Moderate vesicularity	No welding	Lava; red scoriae
Vulcanello 1D	Planar	Massive	Bombs	Fluidal shape	Moderate vesicularity	Moderate to dense welding	No lithics
Vulcanello 2 Lithosome							
Vulcanello 2	Planar, local lenticular	Massive (base), normal to reversely graded	Coarse ash to bombs	Highly elongated clasts	High vesicularity	No welding	Lava; red scoriae
Vulcanello 3 Lithosome							
Vulcanello 3A	Stratified to thinly stratified	Massive	Fine ash	Irregular	–	No welding	–
Vulcanello 3B	Planar to lenticular; aa-lava morphology	Massive	–	–	–	–	–
Vulcanello 3C	Stratified to thinly stratified	Massive, impact structures	Fine ash, sporadic lapilli and bombs	Irregular	–	No welding	Altered lava and scoriae
Vulcanello 3D	Planar, locally lenticular	Massive; normal graded	Coarse lapilli to bombs	Irregular	Moderate vesicularity	No welding	Altered lava and scoriae
Vulcanello 3E	Stratified to densely stratified	Massive, impact structures	Fine ash, sporadic lapilli and bombs	Irregular	–	No welding	Altered lava and scoriae
Vulcanello 3F	Planar to lenticular; aa-lava morphology	Massive	–	–	–	–	–

Table_4

	Volume (km^3, DRE)
Vulcanello 3 cone	0.000025
Valle dei Mostri + Roveto lava flow	0.003
Vulcanello 2 cone	0.0015
Vulcanello 2 submarine lava field	0.245
Vulcanello 1 cone	0.002
Vulcanello 1 lava platform	0.026

	Lava volume/Total volume
Vulcanello 3 lithosome	0.99
Vulcanello 2 lithosome	0.99
Vulcanello 1 lithosome	0.93

Table_5

Unit Sample	Vulcanello 1A V1A	Vulcanello 1B V1B	Vulcanello 1C V1C	Vulcanello 2 V2	Vulcanello 3D V3D
SiO_2 (wt%)	51.79	52.54	52.54	52.61	57.23
TiO_2	0.67	0.65	0.66	0.59	0.56
Al_2O_3	15.33	16.23	15.29	17.11	15.80
$Fe_2O_{3\,T}$	8.74	8.38	8.71	7.29	7.12
MnO	0.14	0.15	0.15	0.13	0.14
MgO	4.18	4.03	4.59	3.31	3.07
CaO	8.14	7.67	8.56	9.11	5.72
Na_2O	3.66	3.83	3.58	3.89	3.95
K_2O	4.57	5.08	4.88	4.89	5.52
P_2O_5	0.45	0.45	0.43	0.41	0.38
L.O.I.	1.98	0.78	0.33	0.32	0.39
sum	99.65	99.79	99.72	99.66	99.86
alkali sum	8.23	8.91	8.46	8.78	9.47
Quartz	-	-	-	-	-
Albite	17.6	16.3	14.9	13.9	32.0
Anorthite	11.9	12.1	11.2	14.8	9.1
Orthoclase	27.0	30.0	28.8	28.9	32.6
Nepheline	7.2	8.7	8.3	10.3	0.7
Diopside	21.2	19.1	23.5	23.7	13.9
Olivine	8.3	8.5	8.2	4.6	7.4
Ilmenite	1.3	1.2	1.2	1.1	1.7
Magnetite	1.3	1.2	1.3	1.7	1.0
Apatite	1.0	1.0	1.0	0.9	0.9

Table_6

Sample	V1B	V1B	V1B	V1B	V1B	V1C	V1C	V1C	V2	V2	V2	V2	V2	V3D	V3D	V3D	V3D	V3D
Inclusion	1	3	4	5	6	1	4	5	1d	4d	1p	2p	4p	1	2	3	4	5
SiO_2 wt%	53.35	54.94	53.75	55.44	55.87	52.10	52.61	51.12	53.29	55.48	54.73	56.77	54.66	61.66	59.50	59.95	59.89	56.33
TiO_2	0.64	0.58	0.65	0.58	0.71	0.66	0.63	0.64	0.60	0.60	0.66	0.58	0.59	0.58	0.57	0.60	0.40	0.61
Al_2O_3	18.16	17.84	17.77	17.74	17.16	17.12	18.02	16.34	17.33	18.24	18.36	16.87	17.83	17.24	17.23	17.17	17.35	19.07
FeO_T	7.37	6.69	7.46	6.81	6.62	8.49	7.77	9.32	6.65	6.84	6.92	6.47	6.70	5.08	5.23	5.18	5.06	4.91
MnO	0.16	0.15	0.15	0.15	0.16	0.17	0.15	0.19	0.15	0.16	0.15	0.14	0.15	0.12	0.11	0.12	0.11	0.10
MgO	2.17	1.92	2.22	1.71	1.80	2.91	2.82	4.26	1.83	1.83	1.74	1.79	1.99	0.96	1.09	1.10	1.13	1.22
CaO	4.91	4.00	5.12	3.62	3.77	6.52	6.05	5.55	3.66	3.88	3.85	3.79	4.09	2.49	3.05	2.77	2.96	3.66
Na_2O	4.79	5.23	4.74	5.14	4.96	4.15	4.57	4.25	5.00	4.71	4.66	5.18	4.52	4.74	5.43	5.35	4.42	4.65
K_2O	6.71	7.09	6.63	7.11	7.00	5.77	6.10	5.70	7.09	7.09	7.25	7.18	7.02	5.13	7.20	6.21	7.37	7.30
P_2O_5	0.60	0.59	0.57	0.55	0.78	0.81	0.56	0.81	0.63	0.60	0.59	0.57	0.59	0.30	0.43	0.29	0.59	0.36
S	0.03	0.01	0.04	0.02	0.02	0.03	0.05	0.04	0.01	0.02	0.02	0.02	0.02	0.01	0.02	0.02	0.02	0.03
Cl	0.31	0.29	0.32	0.33	0.33	0.31	0.30	0.31	0.27	0.31	0.32	0.29	0.29	0.37	0.37	0.41	0.31	0.31
F	0.12	0.16	0.14	0.12	0.13	0.14	0.13	0.13	0.14	0.18	0.14	0.19	0.16	0.12	0.15	0.12	0.12	0.14
H_2O	0.69	0.09	0.65	0.57	0.60	0.88	1.32	0.64	0.69	0.36	0.49	0.35	0.88	0.12	0.38	0.95	0.83	0.42
Total	100.02	99.59	100.22	99.87	99.86	100.05	101.07	99.28	97.33	100.3	99.90	100.18	99.49	98.92	100.4	100.24	100.55	99.11
Fo host	67.97	68.27	68.81	68.25	67.73	70.14	68.28	68.43	69.5	68.91	68.51	70.23	68.34	65.14	64.73	64.53	64.45	69.39
Mg#	0.39	0.39	0.4	0.36	0.37	0.41	0.45	0.51	0.38	0.37	0.36	0.38	0.39	0.29	0.32	0.32	0.33	0.33
Composition corrected for post-entrapment crystallization																		
% ol added	0.0	0.1	0.0	1.2	0.3	0.0	0.0	0.0	0.9	0.9	1.3	1.1	0.0	1.6	1.0	0.8	0.5	1.2
SiO_2 wt%	53.33	55.15	53.63	55.29	55.88	52.07	52.05	51.50	54.59	55.16	54.54	56.44	54.93	61.91	58.82	59.6	59.43	56.6
TiO_2	0.64	0.58	0.65	0.58	0.7	0.66	0.63	0.64	0.61	0.59	0.65	0.57	0.6	0.58	0.56	0.6	0.4	0.61
Al_2O_3	18.16	17.90	17.73	17.54	17.13	17.11	17.83	16.46	17.64	18.03	18.14	16.66	17.92	17.15	16.93	16.98	17.16	19.00
FeO_T	7.37	6.74	7.45	7.09	6.7	8.48	7.66	9.39	7.03	7.01	7.21	6.69	6.7	5.59	5.46	5.38	5.17	5.25
MnO	0.16	0.15	0.15	0.15	0.16	0.18	0.15	0.19	0.15	0.16	0.15	0.14	0.15	0.12	0.11	0.12	0.11	0.1
MgO	2.17	1.96	2.21	2.08	1.89	2.91	2.79	4.29	2.17	2.11	2.15	2.15	1.998	1.44	1.38	1.34	1.27	1.62
CaO	4.91	4.01	5.11	3.58	3.76	6.51	5.98	5.59	3.71	3.83	3.8	3.74	4.11	2.48	3.00	2.74	2.92	3.64
Na_2O	4.79	5.24	4.73	5.08	4.95	4.15	4.52	4.28	5.08	4.66	4.6	5.11	4.54	4.71	5.34	5.29	4.38	4.63
K_2O	6.70	7.12	6.62	7.03	6.98	5.76	6.03	5.74	7.21	7.01	7.17	7.09	7.05	5.105	7.07	6.14	7.29	7.28
P_2O_5	0.60	0.59	0.57	0.54	0.75	0.82	0.56	0.81	0.65	0.59	0.59	0.56	0.6	0.30	0.43	0.29	0.58	0.36
S	0.04	0.02	0.04	0.02	0.02	0.03	0.05	0.04	0.01	0.02	0.02	0.02	0.02	0.01	0.02	0.02	0.02	0.03
Cl	0.32	0.3	0.32	0.33	0.33	0.31	0.3	0.31	0.28	0.31	0.32	0.29	0.29	0.37	0.36	0.41	0.30	0.31
F	0.13	0.17	0.14	0.12	0.13	0.14	0.13	0.14	0.15	0.18	0.14	0.19	0.16	0.12	0.15	0.12	0.12	0.14
H_2O	0.69	0.09	0.65	0.58	0.62	0.88	1.32	0.63	0.72	0.36	0.5	0.36	0.89	0.12	0.39	0.98	0.85	0.43
Total	100.00	100.00	100.00	100.00	100.00	100.00	100.00	100.00	100.00	100.00	100.00	100.00	100.00	100.00	100.00	100.00	100.00	100.00
Mg#	0.39	0.39	0.39	0.38	0.40	0.40	0.45	0.51	0.41	0.40	0.40	0.41	0.40	0.36	0.35	0.35	0.35	0.40
P (MPa)	7.3	0.2	6.4	5.2	5.9	10.6	21.2	6.0	7.6	2.4	4.1	2.3	11.0	0.4	2.7	12.5	10.0	3.2

Table_7

Sample Fragment	V2p V2p2	V2p V2p3	V2p V2p4	V2p V2p5
SiO_2 wt%	54.76	54.86	56.41	56.37
TiO_2	0.63	0.63	0.66	0.66
Al_2O_3	17.37	17.58	17.88	17.68
FeO_T	6.59	6.66	7.00	6.66
MnO	0.13	0.14	0.15	0.16
MgO	1.84	1.84	1.93	1.94
CaO	4.18	4.19	4.37	4.35
Na_2O	4.96	4.85	3.8	4.6
K_2O	6.99	6.97	5.47	6.46
P_2O_5	0.61	0.6	0.65	0.63
S	0.02	0.02	0.02	0.02
Cl	0.31	0.31	0.33	0.33
F	0.17	0.11	0.14	0.11
Total	98.56	98.76	98.82	99.97
H_2O	0.43	0.26	0.34	0.42
Mg#	0.33	0.33	0.33	0.34
P (MPa)	3.2	1.4	2.1	3.0

Table 7

Supplementary Material_text
Click here to download Supplementary Material: Methods.doc

Supplementary Material_figureM1
Click here to download Supplementary Material: Figure M1.jpg

Supplementary Material_figureM2
Click here to download Supplementary Material: Figure M2.jpg